Gas Breakdown by Dielectric Resonator Arrays for Reconfigurable Plasma Metamaterials

A thesis submitted by

Stephen Dennison

in partial fulfillment of the requirements for the degree of

Master of Science

in

Electrical Engineering

Tufts University

May 2017

Adviser: Jeffrey Hopwood

Abstract

Arrays of dielectric resonators—illuminated by an antenna—are used to ignite and sustain multiple microwave plasmas in parallel. A reconfigurable metamaterial could be developed with dielectric resonators providing negative permeability and plasma providing controllable negative permittivity. To generate plasma, cylindrical resonators of calcium titanate were arranged in a linear array with separation distances between 0.5 and 5 mm. The operating frequency was near the HEM_{111} resonance of 1.1 GHz. Sustaining of argon plasma between 0.5 Torr and 1 atm within the array is found to alter the electromagnetic scattering from the dielectric resonators. A relationship was discovered between permittivity and the strength of the coupled electric field. Experimentally, breakdown did not occur for dielectric resonators with low (<40) or high (>800) relative permittivity. Field simulations show a broad maximum in the microwave field generated on the external boundary of the resonators, peaking around $\epsilon_r \sim 200$.

Acknowledgements

I would like to thank my family for their continued support, Adam, Alan, José, and Stephen for their guidance in the lab, and Nick and Yennie for helping me stay steady on the path.

I would also like to thank Professors Lasser, Miller, Sonkusale, and Vandervelde.

There are many others who assisted in valuable ways, but Miriam and Jenn made my life far easier and deserve a special mention.

Finally, thank you to Professor Hopwood for five years of mentorship, guidance, and inspiration.

Table of Contents

Table of Figures

1. Introduction

1.1 Motivation

Metamaterials are composite materials with wave-bending properties that come from the construction and arrangement of their constituent elements. Since metamaterials depend on the structure and the resonances of their components, many metamaterials are built for one mode of operation and cannot be controlled or reconfigured once they are built. For example, electromagnetic metamaterials obtain an overall negative index of refraction by fastening together rigid arrays of split ring resonators and thin wires, which provide negative permeability and permittivity, respectively [1] [2] [3]. If the split ring resonators are used to generate plasma, which can provide negative permittivity and disappears when it is "turned off," switching behavior has been added to the metamaterial [4]. In addition, controlling the properties of the plasma will allow for reconfiguring the entire metamaterial.

Going one step further, if the split ring resonators can be replaced with dielectric resonators, and those dielectric resonators can ignite plasma, then the resulting metamaterial structure will not only be controllable, but made of insulators when it is not in use. This all means that the practical goal of this research was to generate plasma using dielectric resonators, with the intention of using this knowledge to create a reconfigurable metamaterial. If arrays of dielectric resonators ignite and sustain microplasma, the resonators and wires of a classic metamaterial could be

replaced with an all-dielectric system controlled with the application of microwave power.

1.2 Overview

This thesis describes metamaterials, microplasma, and dielectric resonators in greater detail, discusses current reconfigurable metamaterials and plasma metamaterials, and then explains the experimental procedures. The dielectric material chosen for these experiments, calcium titanate, will be discussed as well. Simulations and experimental results will show the conditions for achieving dielectric breakdown. Then, the results of modulating of the electromagnetic scattering of the dielectric resonator array are discussed. Finally, a study is presented on how the permittivity of the dielectric resonators affects the electric field and insight is offered towards future work.

2. Background

This chapter explains how plasma can be used as an element of reconfigurable metamaterials and how plasma could be generated with arrays of dielectric resonators. I first describe metamaterials, plasma, and dielectric resonators so I can discuss plasma reconfigurable metamaterials and the motivations and challenges faced while studying these materials. The final section of the chapter discusses related works on reconfigurable metamaterials and summarizes the current state of the art.

2.1 Metamaterials

Metamaterials are structures that are engineered to have electromagnetic properties that cannot be found in nature. All material can be thought of as matter organized so that the total structure has different properties than its elements. We perceive a continuous material rather than their constituent atoms and molecules. Following this train of thought, a metamaterial is a material where the elements in its structure give it electromagnetic properties not present in any individual element. In other words, just as materials are made up of atoms and molecules but have properties beyond those of the molecules, metamaterials are made up of otherwise conventional materials and behave differently overall compared to those materials [5].

In general, metamaterials are constructed from resonant elements. Resonators will be described in further detail in Chapter 2.3, but for the purposes of this subchapter, a resonator is something that oscillates at certain resonant frequencies more than

other frequencies. The resonators used in metamaterials are on a scale where the characteristic dimension a of an element is smaller than the wavelength λ of the target resonant frequency ω.

$$a \ll \lambda = \frac{2\pi c_0}{\omega} \qquad \textit{Equation 1}$$

This wavelength-to-element size relationship is important because we are interested in the overall properties of the materials and want to guarantee that we are working with a relatively homogenous material at the appropriate scale [1]. Electromagnetic metamaterials (as distinguished from other metamaterials such as acoustic or seismic) are concerned with the characteristic quantities of electromagnetic matter: permittivity and permeability. Before explaining the basic physics of a metamaterial, I must explain where these quantities come from and how they are related to the propagation of electromagnetic waves.

The electric permittivity or dielectric constant, ε, of a material, is a way to measure how electric field behaves in a material as compared to free space. Relative permittivity is written as $\varepsilon_r = \varepsilon/\varepsilon_0$, where $\varepsilon_0 = 8.85\times10^{-12}F/m$ is the permittivity of free space. The magnetic permeability, μ, of a material, is analogous for magnetic fields. The relative permeability, $\mu_r = \mu/\mu_0$, where $\mu_0 = 4\pi\times 10^{-7}H/m$, describes the magnetization properties of the material. The speed of light (or any electromagnetic wave) in any material can be found by relating c to the quantities ε_r and μ_r [6].

These relationships between permittivity, permeability, and electromagnetic waves come from Maxwell's equations, which govern classical electromagnetism.

Maxwell's equations for the curls of $\boldsymbol{B}$ and $\boldsymbol{E}$, the magnetic and electric fields in free space in the absence of current but with conductivity σ, are as follows:

$$\nabla \times \boldsymbol{E} = -\frac{\partial \boldsymbol{B}}{\partial t} \qquad \textit{Equation 2}$$

$$\nabla \times \boldsymbol{B} = \mu\sigma\boldsymbol{E} + \epsilon\mu\frac{\partial \boldsymbol{E}}{\partial t} \qquad \textit{Equation 3}$$

Note that the permittivity and permeability of free space appear in Equation 3, which says that an electric field changing in time creates a curl in the magnetic field. Taking the curl of these curls, we can decouple magnetic and electric fields to derive wave equations:

$$\nabla^2 \boldsymbol{E} = \epsilon\mu\frac{\partial^2 \boldsymbol{E}}{\partial t^2} + \mu\sigma\frac{\partial \boldsymbol{E}}{\partial t} \qquad \textit{Equation 4}$$

$$\nabla^2 \boldsymbol{B} = \epsilon\mu\frac{\partial^2 \boldsymbol{B}}{\partial t^2} + \mu\sigma\frac{\partial \boldsymbol{B}}{\partial t} \qquad \textit{Equation 5}$$

These are wave equations where permittivity and permeability are the reciprocal of the square of the speed of light. Electromagnetic waves travel in free space at the speed of light, which is defined with the product of permeability and permittivity: $c = 1/\sqrt{\mu_0\epsilon_0} = 3{\times}10^8 m/s$. These waves, solutions of a second order differential equation, take the form $Ae^{-j\phi} = Ae^{-j(\tilde{\boldsymbol{k}}z-\omega t)}$, a complex exponential of frequency ω that can either propagate or decay depending on the medium. A, the amplitude, can be either a magnetic or electric field component, and $\phi = -(\omega t - \boldsymbol{k}\cdot z)$ captures how fast the wave oscillates in time and how it behaves in space. At a far distance from their source, these become plane waves. In matter, the magnetic and

electric behavior of waves changes in a way that can be captured by these expressions of permittivity and permeability. I discuss permittivity in greater detail in Chapter 2.3.

More generally, we can understand how these waves propagate in isotropic matter by Equation 6, the dispersion relation, which shows another relationship between some of the quantities introduced above if k is completely real:

$$k^2 = \frac{\omega^2}{c^2} n^2 \qquad \textit{Equation 6}$$

ω is a monochromatic angular frequency and k is the real wave vector, introduced above in the ϕ term:

$$k = \frac{2\pi}{\lambda} \qquad \textit{Equation 7}$$

The wave vector captures how much a wave changes relative to its wavelength and which direction it is traveling in. The magnitude of k is called the spatial angular frequency, or wavenumber, and captures oscillations per unit of space, but the direction of k points in the direction of the propagation and phase velocity. Phase velocity describes how "fast" a fixed point on a wave, such as a peak or trough, travels through space, and changes based on frequency for a medium. Phase velocity is the angular frequency divided by the wave vector:

$$v_{phase} = \frac{\omega}{k} \qquad \textit{Equation 8}$$

The group velocity is the partial derivative of the angular frequency with respect to the wave vector, and captures how fast "groups" of waves travel. Dispersion

relations allow us to describe not only how fast information travels, but what it looks like and how fast it changes.

The dispersion equation helps explain, for example, why different wavelengths of light (monochromatic colors) diverge at different speeds in a prism. This is because when electromagnetic waves cross the interface of two different materials, the waves refract or "bend" in the second medium. How much the light bends is captured by the index of refraction, which is written as n in Equation 6 and can be calculated with a material's relative permittivity and permeability:

$$n = \sqrt{\frac{\varepsilon\mu}{\epsilon_0\mu_0}} = \sqrt{\epsilon_r}\sqrt{\mu_r} \qquad \textit{Equation 9}$$

The index of refraction determines how much of an electromagnetic wave is transmitted or reflected when the wave passes the boundary between two materials. In Figure 1, an incident wave is shown reflecting and refracting through the boundary of two media. The refractive index of a material can also be written as $n = \pm\sqrt{\varepsilon_r\mu_r}$, where ϵ_r and μ_r are the relative permittivity and relative permeability, respectively, of the material, and the sign outside the square root is only negative if both quantities are negative.

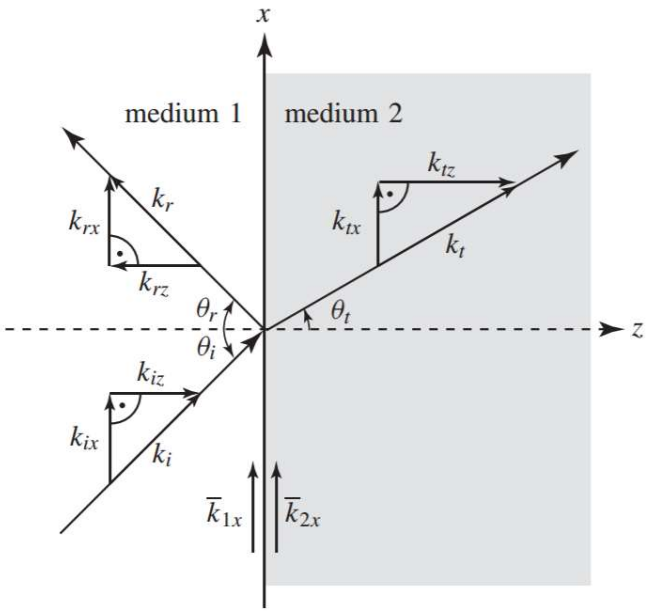

Figure 1: Mapping reflection and transmission or refraction at the boundary between two media. θ_i, θ_r, and θ_t are incident, reflected, and refracted angels of the wave [5].

Conventional materials have a positive index of refraction due to having positive permeability and permittivity. If a material has either negative permeability or permittivity, then n is a negative square root and waves cannot propagate through the material. However, if both ϵ and μ are negative, then n is negative, but real, and waves can propagate. Figure 2 is a plot of ϵ and μ, demonstrating that propagation only occurs if ϵ and μ have the same sign.

In addition, if the conductivity is introduced as in Equation 3, $\tilde{k}$ is a complex quantity, and the wave equation contains an extra exponential term that further decays the amplitude of the traveling wave. As a result, waves propagate if both ϵ and μ are the same sign, and decay if the material has conductive or dissipate behavior that can attenuate a wave even if it propagates.

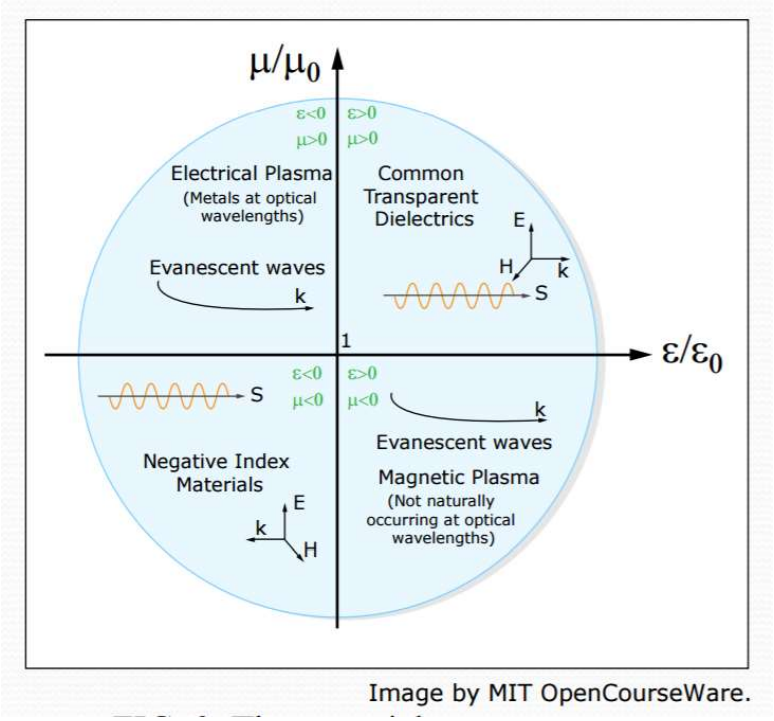

Figure 2: Propagation and index of refraction. The material is transparent if both mu and epsilon are positive valued. If either value is negative, waves evanesce and the material is opaque. However, quadrant III shows that if both mu and epsilon are negative, the material is transparent and can propagate waves. *[7]*

In 1964, V. G. Veselago demonstrated the physics of a material that had both negative permeability and permittivity. His paper on the subject began the study of these materials. When both μ and ϵ are negative, n is called a negative index of refraction, and the material is said to be left-handed (to distinguish it from conventional materials that follow a "right handed" orthogonal relationship between the wave vector and electric and magnetic fields). Both the terms "left handed material" (abbreviated LHM) and "negative index of refraction" refer to metamaterials. Veselago's paper demonstrated that the directionality of many physical phenomena is swapped, as seen in Figure 3 and Figure 4.

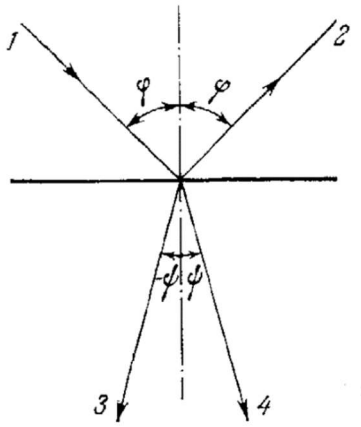

Figure 3: Passage of a ray through the boundary between two media. 1 – incident ray; 2 – reflected ray; 3 – reflected ray if the second medium is left-handed; 4- refracted ray if the second medium is right-handed [8].

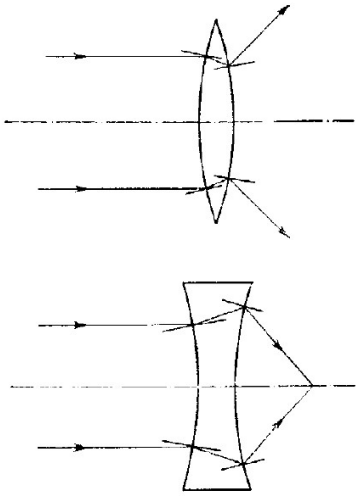

Figure 4: Light refracting through lenses made of left-handed materials. Note that a convex lens diverges and a concave converges [8].

In addition to modifying Snell's law and many optical properties, left-handed material has implications for the transport of energy and the wave vector. In a LHM, the wave vector $\boldsymbol{k}$ opposes the Poynting vector, which capture the energy of the wave and conventionally points in a right-handed fashion perpendicular to both the electric and magnetic fields.

$$\boldsymbol{S} = \frac{1}{\mu}(\boldsymbol{E}\times\boldsymbol{B}) \qquad \textit{Equation 10}$$

Due to the right-hand rule and the vector cross product in the definition, $\boldsymbol{S}$ is typically orthogonal to both $\boldsymbol{E}$ and $\boldsymbol{B}$. When $\boldsymbol{k}$ opposes the direction $\boldsymbol{S}$, as can happen with a LHM, waves appear to propagate from a source when work is being done on it, and convex lenses diverge while concave lenses converge [8].

Since his paper was theoretical, Veselago did not build a material with these properties or demonstrate them experimentally, despite suggesting some materials with negative permeability or permittivity. Notwithstanding the often-made claim that negative permeability and permittivity do not occur in nature, there are many recorded instances of materials with these properties. Some metals like gold and silver have negative permittivities at optical frequencies. As will be discussed later, plasma has negative permittivity at frequencies below its electron plasma frequency. Negative permeability can be found in ferrimagnetic materials (ferrites) [5]. However, this thesis is chiefly concerned with negative-index material in microwave regimes.

Although the theoretical background existed, experimental research on metamaterials did not begin in earnest until 1999 when Pendry suggested and modeled the split ring resonator (SRR) medium. A split ring resonator is, as the name suggests, a resonator in the shape of a ring that is not completely closed. Pendry introduced the SRR as an example of a non-magnetic material with overall magnetic properties of negative permeability. He described, without conducting experiments, how enhancing the discontinuities and capacitances of his theorized structure allowed him control over the overall permeability [1].

The effective permeability of a SRR can be described with the following equation:

$$\mu_{eff}(\omega) = 1 - \frac{F\omega^2}{\omega^2 - \omega_0^2 + i\omega\Gamma}$$ *Equation 11*

Where F is the fractional area ($\frac{\pi r^2}{a^2}$) of the unit cell occupied by the interior of the split ring, Γ is the dissipation factor, and ω_0 is the resonant frequency, derived from some more parameters left out for clarity [2]. This is a second order system with poles when $\omega = \omega_0$. At these poles, the denominator of the second term becomes very small, making the whole second term much larger than one. The permeability of the split ring resonator arrays becomes negative at these resonances.

Figure 5 shows the frequency response near resonance of a split ring resonator developed by D. R. Smith *et* al. This SRR consists of two concentric rings with a width *c* and a separation *d* on a substrate. The split in the rings allows the structure to resonate at larger wavelengths than the expected half-wave frequency because a closed ring would require half-length multiples for resonance. The second ring in the SRR increases the capacitance of the whole structure, which lowers the resonant frequency and concentrates the electric field [2].

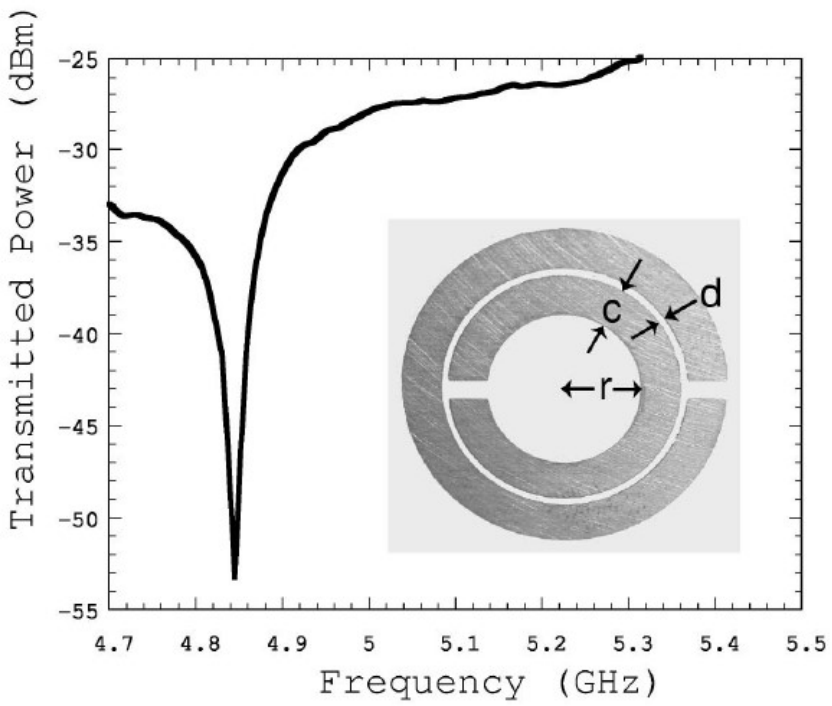

Figure 5: Transmission of split ring resonator developed by D. R. Smith et al. *around the resonant frequency [2]*

Smith then combined SRR columns with periodically placed thin wires of conductive material. The effective dielectric function of the conductive wires is negative at frequencies below the resonant frequency, ω_p:

$$\epsilon_{eff}(\omega) = 1 - \omega_p^2/\omega^2 \qquad \textit{Equation 12}$$

This resonant frequency is also called the plasma frequency, and can be proved to have the general form:

$$\omega_p = \frac{1}{\sqrt{d^2 L \epsilon_0}} \qquad \textit{Equation 13}$$

Where d is the radius and L is the self-conductance per unit length [2].

By combining these two resonating materials that achieve negative properties at similar resonances, propagation can be achieved. Figure 6 shows the "classic"

metamaterial structure with alternating SRR's and conducting wires, which can provide a negative index of refraction.

Figure 6: Split ring resonator array with metal wire array interspersed [9].

Figure 7 shows that while SRR's have a band of poor transmission near resonance, with the addition of the proper conducting wires, this region of negative permittivity can be transformed into a band pass region. Waves cannot propagate through the SRR medium when permeability is negative, in the narrow band of resonance where this occurs, and cannot propagate through the wire medium below the resonant plasma frequency. However, propagation with a negative index of refraction is possible when the two materials are combined and their resonance bands overlap.

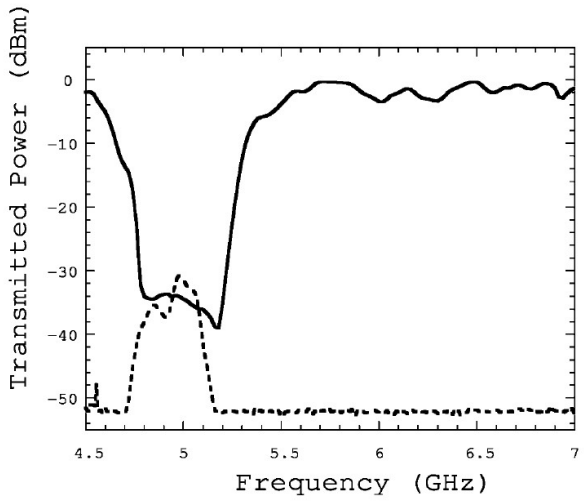

Figure 7: Solid curve shows transmission of just SRR array, with band gap of low transmission around 5 GHz. Dashed curve shows transmission when combined with metallic conducting poles, with a bandpass region at 5 GHz instead [2]

Since the construction of this initial metamaterial, there have been years of study on materials of many kinds and with several properties, but the fundamentals remain that one must combine resonant materials that have exceptional properties at resonance.

In the previous example of a metamaterial, and in many other constructions, both kinds of resonators (split rings and thin wires) were made of metal and were conductive. This point will be discussed later for the purposes of cloaking.

The equation for intrinsic impedance of a medium is:

$$\eta = \frac{\omega\mu}{k} = \sqrt{\mu/\epsilon} \qquad \textit{Equation 14}$$

And for free space, [10]

$$\eta_0 = \sqrt{\mu_0/\epsilon_0} = 377\Omega \qquad \textit{Equation 15}$$

If a material can be impedance matched to free space, this could be one way to achieve "perfect" absorption of electromagnetic radiation. Minimizing reflection is a desirable goal for developing cloaking technology.

Finally, due to narrow resonances, metamaterials often only offer their unusual behavior over a small band. This partially motivates the desire to tune or reconfigure a metamaterial. In addition, while semiconductor circuits can operate in low frequencies (<1 GHz), lasers can transmit information in the infrared and visible spectrum (>300 THz), and waveguides can bridge some of the gap at microwave frequencies (300 MHz to 300 GHz), there is a band of the electromagnetic spectrum that is under-utilized. This terahertz gap, ranging from 300 GHz to 30 THz, is where currently developed technologies fail to operate to a sufficient degree [11]. Metamaterials may offer a way to operate or manipulate light in the THz range.

2.2 Plasma

This chapter will describe the important properties of plasmas, how plasma can be generated, and how plasma will be used in this project.

As mentioned in the previous subchapter, plasma is one of the few materials that is known to have a negative permittivity "naturally." This, by itself, makes plasma an attractive contender as a component in a metamaterial. Beyond this, since plasma only exists when it has been initiated or "turned on" and disappears once its power source is gone, it offers a potential method to control metamaterials.

Matter can be transformed from one state to another by the application of energy. Just as heating a solid melts the matter into a liquid and heating a liquid causes it to evaporate into a gas, applying energy to a gas transforms it into a plasma.

Plasmas, referred to as the “fourth state of matter,” result from the application of energy to a gas. When sufficient energy is applied, the charge-neutral gas atoms split into charge carrying ions and electrons. Although at first the gas may have uneven amounts of ions and electrons, the plasma eventually enters a steady-state. Breakdown is the stage in plasma generation when the neutral gas begins to transform into charged particles [12]. Figure 8 shows a wide array of plasmas encountered both in space and laboratories.

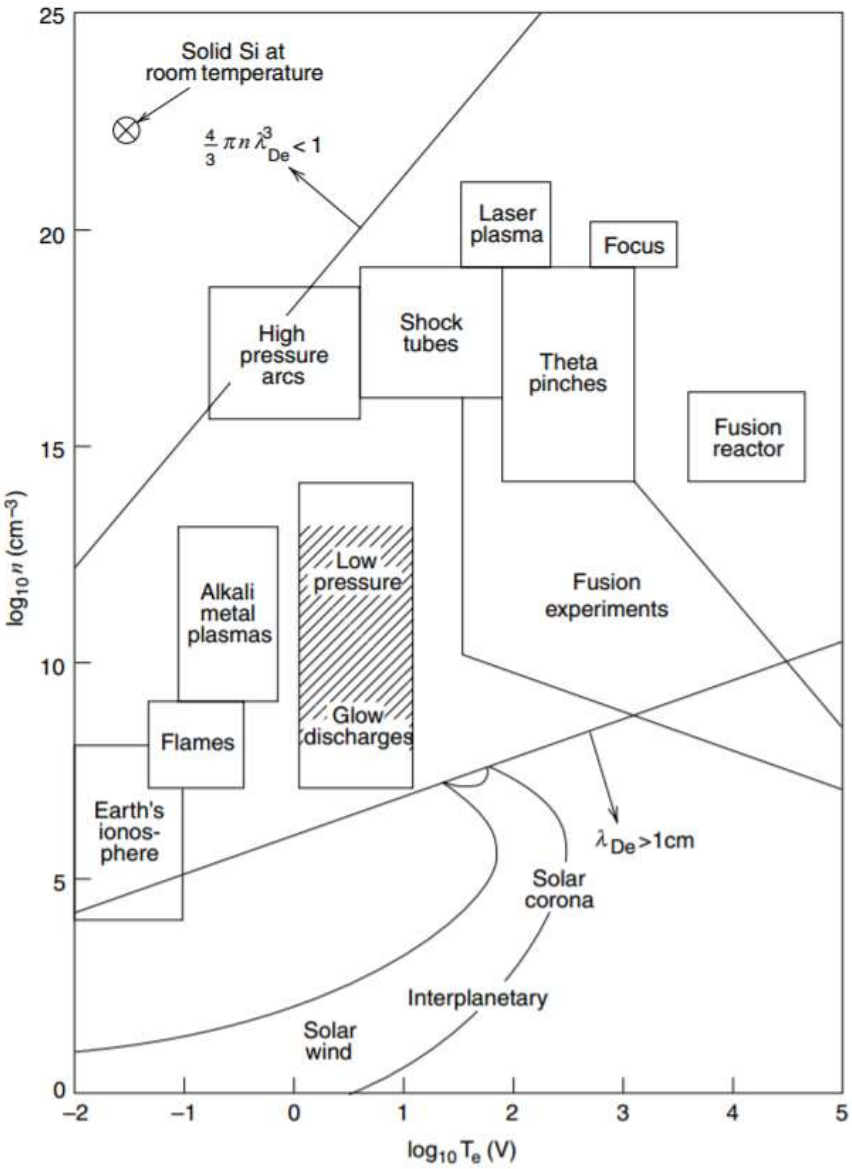

Figure 8: Space and laboratory plasmas on a log n versus log T_e diagram (electron density versus electron temperature) [13] The plasma discussed in this thesis is mostly in the shaded region "Low pressure" and "Glow discharges".

The most important property of a plasma is its electron density, n_e. Plasma is characterized by this quantity, a measure of electrons per unit volume, in addition to particle densities of ions and overall particles [13]. Since electrons drive reactions through their collisions with neutral particles and are the dominant charge carrier due to their low mass, knowing the electron density informs the behavior of

the plasma. For example, electron density is used to calculate the overall permittivity of a plasma.

Other important plasma properties are its temperature and pressure. A "cold" plasma indicates that even though a charge equilibrium has been reached (an equivalent number of electrons and ions), the temperatures of the particles are not in thermodynamic equilibrium, and the ions and neutral particles have a lower temperature than the electrons [13].

The permittivity of plasma responds differently depending on the frequency of the applied field. Permittivity is related to ω_{pe}, the electron plasma frequency, which is the natural frequency of oscillation for electrons in the plasma and defined as:

$$\omega_{pe} = \sqrt{\frac{n_e e^2}{\varepsilon_0 m_e}} \qquad \textit{Equation 16}$$

Where n_e is the electron density, e is the elementary charge of an electron, ϵ_0 is the permittivity of free space, and m_e is the electron rest mass. Since e, ϵ_0, and m_e are constants, $\omega_{pe} \propto \sqrt{n_e}$.

The overall permittivity of plasma can be modeled with Maxwell's equations and the definition of conductivity, $\bar{J} = \sigma \bar{E}$. For high frequency fields, where σ_p is the plasma conductivity and ν_m captures collision frequency, the curl of the magnetic field is related to:

$$\nabla \times \bar{H} = \varepsilon_0 + \frac{\sigma_p}{j\omega} = \varepsilon_0 \left[1 - \frac{\omega_{pe}^2}{\omega(\omega - j\nu_m)}\right] \qquad \textit{Equation 17}$$

At low pressures, collisions can be ignored and the plasma permittivity can be modeled with the Drude model [14]:

$$\varepsilon_r = 1 - \frac{\omega_{pe}^2}{\omega^2} \qquad \textit{Equation 18}$$

This means that when the frequency applied to the plasma is less than the electron plasma frequency, the permittivity is negative. In this sense, plasma "looks" like a conductive metal at frequencies below its electron resonant frequency and like a dielectric material at greater frequencies. Since the plasma frequency depends on electron density, and waves can only propagate through a material with a positive permittivity, the electron density of a plasma determines whether waves will propagate.

At lower frequencies, electrons can move freely enough to cancel out the charge of present electric fields. However, if an incident wave has a higher frequency than the electron plasma frequency, those electrons cannot respond quickly to cancel out an electric field. The wave can pass through and the plasma behaves more like a dielectric or insulating material [13]. This negative permittivity makes plasma an attractive contender as an element in a metamaterial.

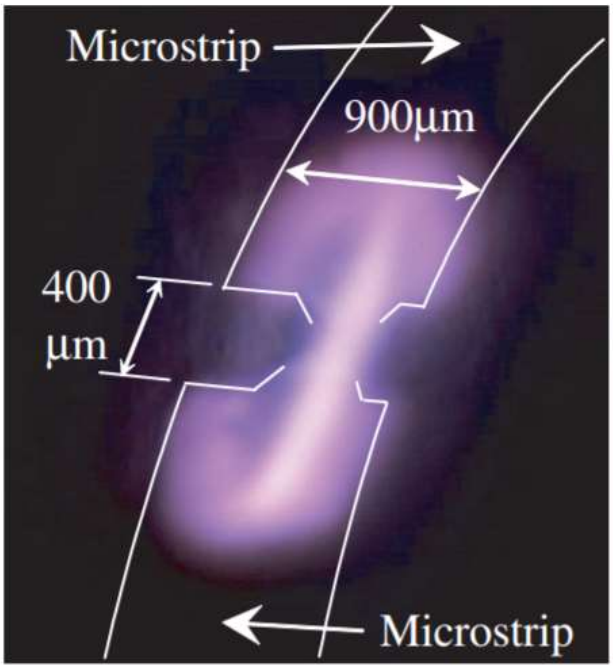

Figure 9: Example of microplasma generated with microstrip resonator in atmospheric pressure at 1 W; the discharge is less than 900 µm wide [15].

Though there are many kinds of plasma, including those found in space and earth's atmosphere, we are concerned with microplasmas. One of example of a microplasma is shown in Figure 9. This term loosely describes plasma discharges smaller than 1 mm in at least one dimension. Their applications and areas of study include "material processing, plasma displays, medical treatment, ozone generation for water treatment, and pollution control." One particularly important use of plasmas is in the fabrication of integrated circuits, where material is deposited in layers onto a substrate through the mechanism called sputtering. In addition to fabricating microelectronics, it is possible that microplasmas can be used in a new class of microelectronics transistors and devices [16].

One common method of applying an electric field to plasma is to capacitively couple the electric field to the gas. A microwave signal is applied between two

electrodes. The electric field between the two contacts begins the breakdown process by accelerating any free electrons up to energies required for ionization of the gas. The ideal separation of the two electrodes depends on the pressure of the gas.

Sputtering is the word used to describe when incoming "energetic particles" knock particles off of a target material. The ions present in a plasma can provide these energetic particles. A substrate can be put in the path of the dislodged particles in order to deposit layers on the substrate. This is an important step in the process of fabricating integrated circuits. However, plasma can also lead to unwanted sputtering, where the metal contacts used to ignite and sustain the plasma, for example, are slowly eroded. Sputtering is the result of high energy ions striking the electrodes, and can be avoided by using high pressure gas or a low-voltage electrode. High pressure makes it more likely that ions will have collisions before they hit the electrodes. Though in some situations, sputtering is the desired result, we do not want to destroy the electrodes or surrounding environment [13]. Fortunately, at high frequencies, sputtering does not occur because the heavier ions do not move as much as the lighter electrons [16].

Microplasmas have many advantages, especially for long-term use. Their small size makes them good candidates for higher frequency applications, as they can satisfy the relationship in Equation 1. Microplasma discharges with microwave frequency resonators require much lower voltages. Microwave discharges are also less likely to generate unwanted sputtering because the heavy ions do not move as much in

the microwave fields. Ions and atoms are “heavy particles” in relationship to the lighter electrons [16].

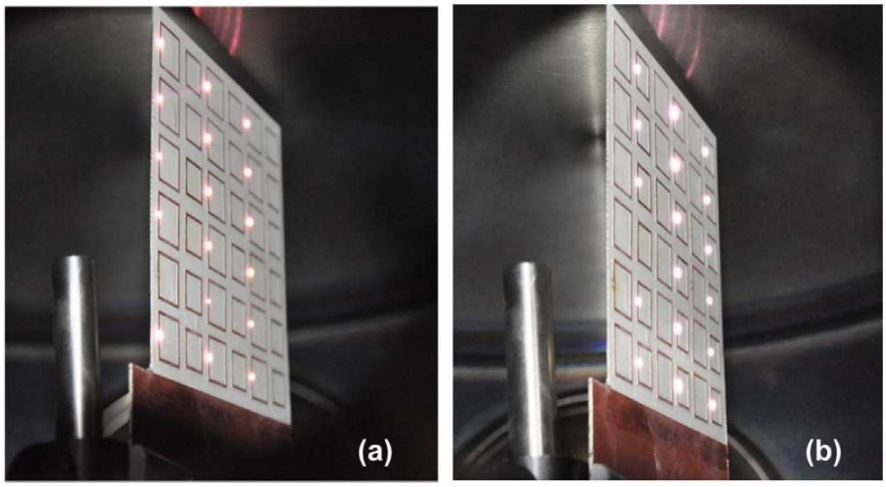

Figure 10: Wireless plasma generation in dual frequency split-ring resonator metamaterial at pressure of 40 Torr. Plasma is only generated in arrays of (a) 2.1 GHz and (b) 2.45 GHz [4].

Since the gap in a split ring resonator causes a potential difference, split ring resonators can be used to start microplasmas [15]. In addition, when power is supplied to one resonator in an array of identical microwave resonators, that power is shared and microplasmas start between the resonators and the ground plane [17].

In a 2014 experiment, Singh et al. achieved breakdown in the gap of split ring resonators at frequencies of 2.1 and 2.45 GHz, as seen in Figure 10. An antenna transmitted power to the array, and at resonance the voltage in the gap was high enough to start a plasma in argon. The experiment demonstrated how plasma could be used as an element in metamaterials, with the split ring resonators providing negative permeability and the plasma providing negative permittivity in a certain frequency band. In addition, this experiment demonstrated one solution of how to

counter the problem of metamaterial narrow band behavior, by creating interlaced arrays of resonating material with different resonant frequencies [4].

A recent study shows that microplasmas started with split ring resonators have nonlinear functions with power, a potential candidate for reconfigurability if incorporated into a metamaterial [18].

2.3 Dielectric resonators

We have now seen conductive resonators and plasma generated with those resonators. In this section, I will describe permittivity, explain dielectric resonators, contrast these with metal resonators, and explore the significance of modes of resonance.

The matter we interact with every day can be grouped into two broad categories: conductors, which allow the free movement of electrons within themselves, and insulators, which have electrons bound to their atoms or molecules. Dielectric is another word for "insulator" [6].

A dielectric does not conduct in the presence of an electric field, but still responds to the application of a field. The electrons inside the atoms either rotate or stretch in response to this electric field in a process called polarization. When permittivity was introduced in Chapter 2.1, I was actually describing the overall polarization of a material. As a reminder, the overall permittivity ϵ of a material can be described as the permittivity of free space ϵ_0 multiplied by the relative permittivity ϵ_r, often called the dielectric constant or function:

$$\epsilon = \epsilon_r \epsilon_0 \qquad \textit{Equation 19}$$

In order to understand how a dielectric can resonate, first a microwave resonator should be explained. For electrical engineers, a resonator circuit consists of an inductance, a capacitance, and a resistance, and can be modeled as an RLC in either series or parallel. At some frequency, the stored magnetic and electric energies will be equal; this frequency is called the resonant frequency, and can be calculated in the lossless case with Equation 20.

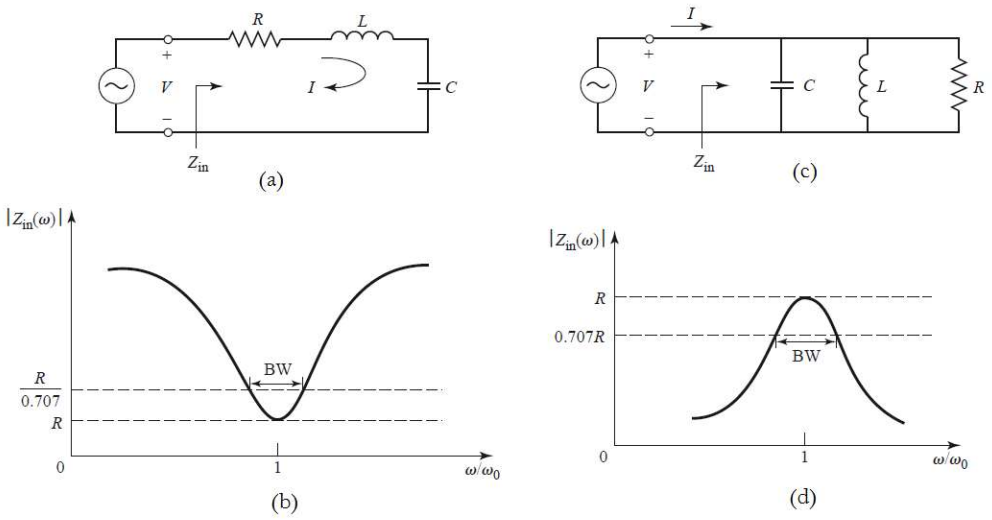

Figure 11: RLC circuits and their normalized frequency responses in (a) series and (c) parallel with responses (c) and (d), respectively [10].

$$\omega_0 = \frac{1}{\sqrt{LC}} \qquad \textit{Equation 20}$$

When a resonator reaches a steady state at resonance, the power entering the system is equal to the power dissipated by the system. This is a way to identify resonators more generally, but also lets us define Q, also called the quality factor, as

$$Q = \omega \frac{average\ energy\ stored}{energy\ loss/second} = \omega \frac{W_m + W_e}{P_{loss}} \qquad \textit{Equation 21}$$

Where W_m is the stored magnetic energy and W_e is the stored electric energy. P_{loss} captures losses due to conductor losses, dielectric losses, and radiation losses. If $R = 0$, the resonant system is said to be unloaded, and we can describe the bandwidth BW of our resonance as follows:

$$BW = \frac{1}{Q_0} = \frac{2\Delta\omega}{\omega_0} \qquad \textit{Equation 22}$$

Where Q_0 is the unloaded quality factor, $\Delta\omega$ is the frequency band to the -3dB magnitude, and ω_0 is the center resonant frequency.

This describes in mathematical language what a resonance means. We have already seen three kinds of resonant materials, split ring resonators, thin wires, and plasma. I will introduce microwave resonators made of waveguides so that I can describe microwave dielectric resonators.

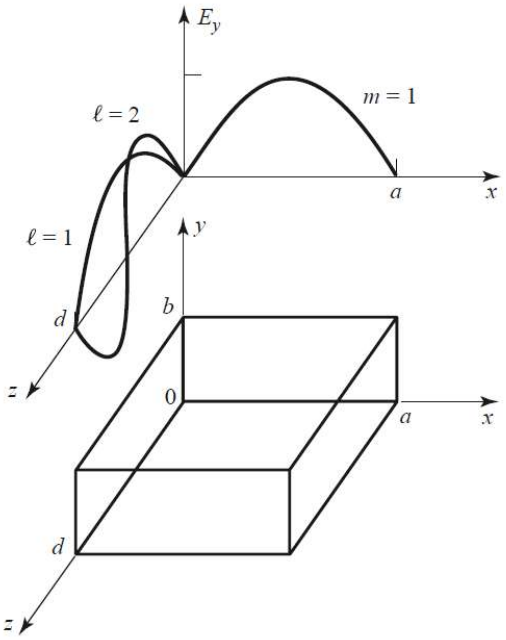

Figure 12: Rectangular cavity waveguide resonator with electric field variations for the TE_{101} and TE_{102} resonant modes [10].

Waveguides are hollow metal tubes used to transport microwaves; they are necessary because wires are inappropriate at the small wavelengths of microwaves, 1 mm to 1 m, due to parasitic losses. If we enclose a rectangular waveguide, we can use it as a resonator if its characteristic dimension is an integer multiple of a half-guided wavelength of the resonant frequency, as shown in Figure 12: Rectangular cavity waveguide resonator with electric field variations for the TE_{101} and TE_{102} resonant modes . In perfect waveguides with perfect conducting surfaces, the electric field is zero at all boundaries, waves will perfectly reflect in the cavity, and there are no losses. Real waveguides have losses, but even taking this into account, waveguide cavity resonators have very high Q's. The resonant frequency of a cavity resonator depends on its three dimensions:

$$f_{mnl} = \frac{ck_{mnl}}{2\pi\sqrt{\epsilon_r\mu_r}} = \frac{c}{2\pi\sqrt{\epsilon_r\mu_r}}\sqrt{\left(\frac{m\pi}{a}\right)^2 + \left(\frac{n\pi}{b}\right)^2 + \left(\frac{l\pi}{d}\right)^2} \qquad \textit{Equation 23}$$

Which is also clear from its wavenumber, k_{mnl}, which explains why modes are quantized by the dimensions of the cavity:

$$k_{mnl} = \sqrt{\left(\frac{m\pi}{a}\right)^2 + \left(\frac{n\pi}{b}\right)^2 + \left(\frac{l\pi}{d}\right)^2} \qquad \textit{Equation 24}$$

Modes only exist as multiples of the dimensions of the waveguide because electric fields must be zero at the walls of the conductor.

The resonant frequency also depends on the permittivity and permeability. Since most material has a permeability of around 1, the resonant frequency of a cavity

resonator can be scaled by $\sqrt{\epsilon_r}$ by inserting dielectric material, allowing lower resonant frequencies at smaller sizes. This is another example of the permittivity capturing how a material affects electromagnetic waves.

These resonant frequencies can be characterized by certain patterns or wave behavior called modes. A mode is called transverse electric (TE) if no electric field component is in the direction of propagation, transverse magnetic (TM) if no magnetic field is in the direction of propagation, and transverse electromagnetic (TEM) if neither field is in the direction of propagation. In rectangular metal waveguides, because E field must be zero at the boundaries, only certain quantized modes are allowed. Propagation can only occur at these frequencies.

In the previous descriptions, the subscripts m, n, l referred to the appropriate dimension, and give a way of identifying or describing a mode.

Waveguide resonators can be made from any geometry, but the calculations for resonance become more complicated. Closing both ends of a cylindrical waveguide turns it into a resonator with a resonant frequency in the TE mode of

$$f_{mnl} = \frac{c}{2\pi\sqrt{\mu_r \epsilon_r}} \sqrt{\left(\frac{p'_{nm}}{a}\right)^2 + \left(\frac{l\pi}{d}\right)^2} \qquad \textit{Equation 25}$$

And in the TM mode of:

$$f_{mnl} = \frac{c}{2\pi\sqrt{\mu_r \epsilon_r}} \sqrt{\left(\frac{p_{nm}}{a}\right)^2 + \left(\frac{l\pi}{d}\right)^2} \qquad \textit{Equation 26}$$

Where a is the radius of the cavity and d is the height as shown in Figure 13. p_{nm} is the m^{th} root of J_n, or $J_n(p_{nm}) = 0$, and p'_{nm} is the m^{th} root of the derivative of

J_n. J_n is the Bessel function of the first kind, the solution that arises from solving Maxwell's equations for $\nabla \times E$ and $\nabla \times H$, partial differential equations in cylindrical or spherical coordinates.

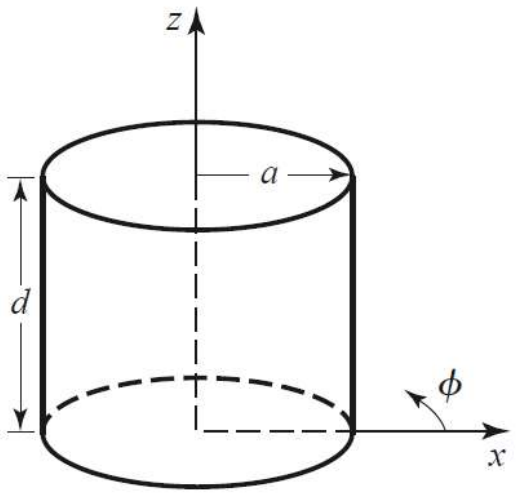

Figure 13: Cylindrical cavity resonator with radius a and height d [10].

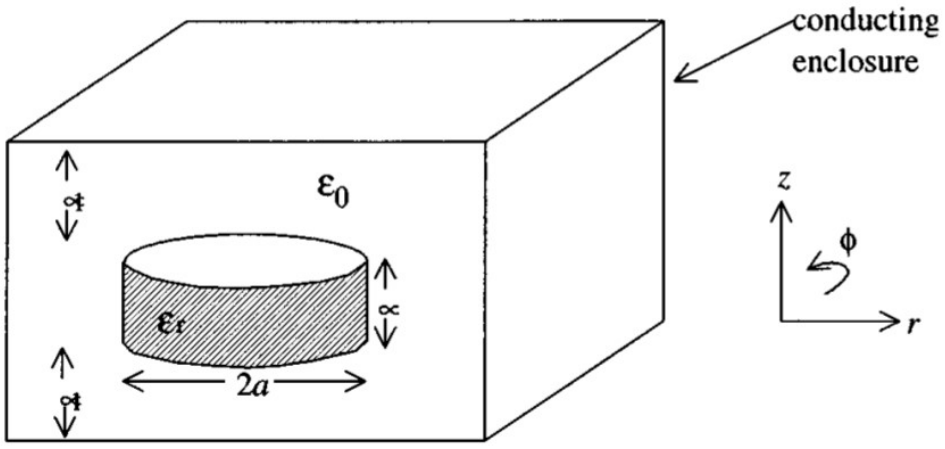

Figure 14: Commonly used dielectric resonator structure. Note the use of cylindrical coordinates [19].

In his seminal 1939 paper, Richtmeyer proved that a ring made of dielectric material could resonate. These dielectric resonators, which can be thought of as waveguides bent so that the electromagnetic wave is more or less confined to the

cylinder itself, can be made in other shapes, commonly cylindrical or spherical. A cylindrical dielectric resonator is essentially equivalent to a cylindrical cavity resonator. It can be modeled as a waveguide open at both ends [20].

Dielectric material is useful for a number of microwave frequency applications, notably as a substrate for microstrip lines and coplanar waveguides. We are particularly interested when the permittivity is relatively high and the loss tangent is low. Dielectric resonators are suitable waveguides at RF applications when metal waveguides have too high conductive losses. Dielectrics are commonly used as compact antennas and filter components for high frequency circuitry. Dielectric resonators can provide a high Q filter [19]. Waveguides can be made from dielectric material instead of perfect conductors, or with dielectric material inserted into the waveguide to achieve propagation of lower frequencies at smaller sizes. Though the fields are no longer tightly confined inside the waveguide, dielectric resonators can propagate waves at much smaller physical size than air-filled waveguides [10].

When tuning and exciting dielectric resonator modes, the two modes that practically resonate are $TE_{01\delta}$ and $HE_{11\delta}$. The δ is used instead of an integer because the z direction does often not contain an integer number of half-wavelengths [21].

Here it is necessary to define electromagnetic scattering, commonly described with the S-parameters of a two-port network. Scattering in general is the process of a particle or wave deviating from its straight path.

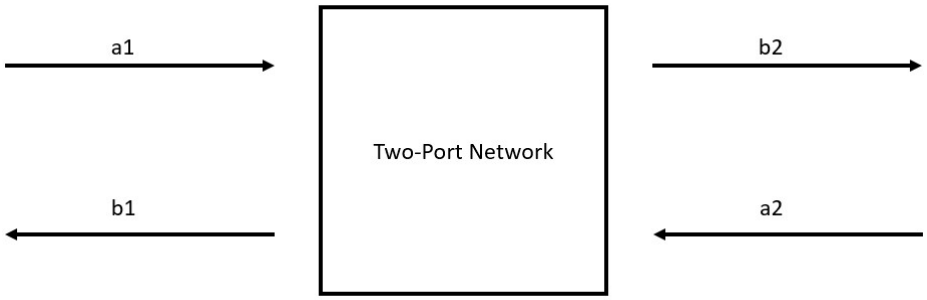

Figure 15: S parameter black box with two inputs and outputs.

We can define the relationships between a's and b's with these equations, also written in matrix form:

$$b_1 = S_{11}a_1 + S_{12}a_2 \qquad \textit{Equation 27}$$

$$b_2 = S_{21}a_1 + S_{22}a_2 \qquad \textit{Equation 28}$$

$$\begin{pmatrix} b_1 \\ b_2 \end{pmatrix} = \begin{pmatrix} S_{11} & S_{12} \\ S_{21} & S_{22} \end{pmatrix} \begin{pmatrix} a_1 \\ a_2 \end{pmatrix} \qquad \textit{Equation 29}$$

S_{11} is the reflection coefficient of the input port. It relates the transmitted power by the antenna to the power that is reflected. S_{21} is the forward gain. It relates the power transmitted by input and the power received by the output [10].

For the purposes of this thesis, a resonance is a frequency where there is a maximum value of Q:

$$Q = \omega \frac{energy\ stored}{power\ radiated} \qquad \textit{Equation 30}$$

This can be indirectly related to our S-parameters, because there will be a dramatic change in our reflection (S_{11}) or transmission (S_{12}) near resonance, which can be seen in an S-parameter plot to resemble a resonance.

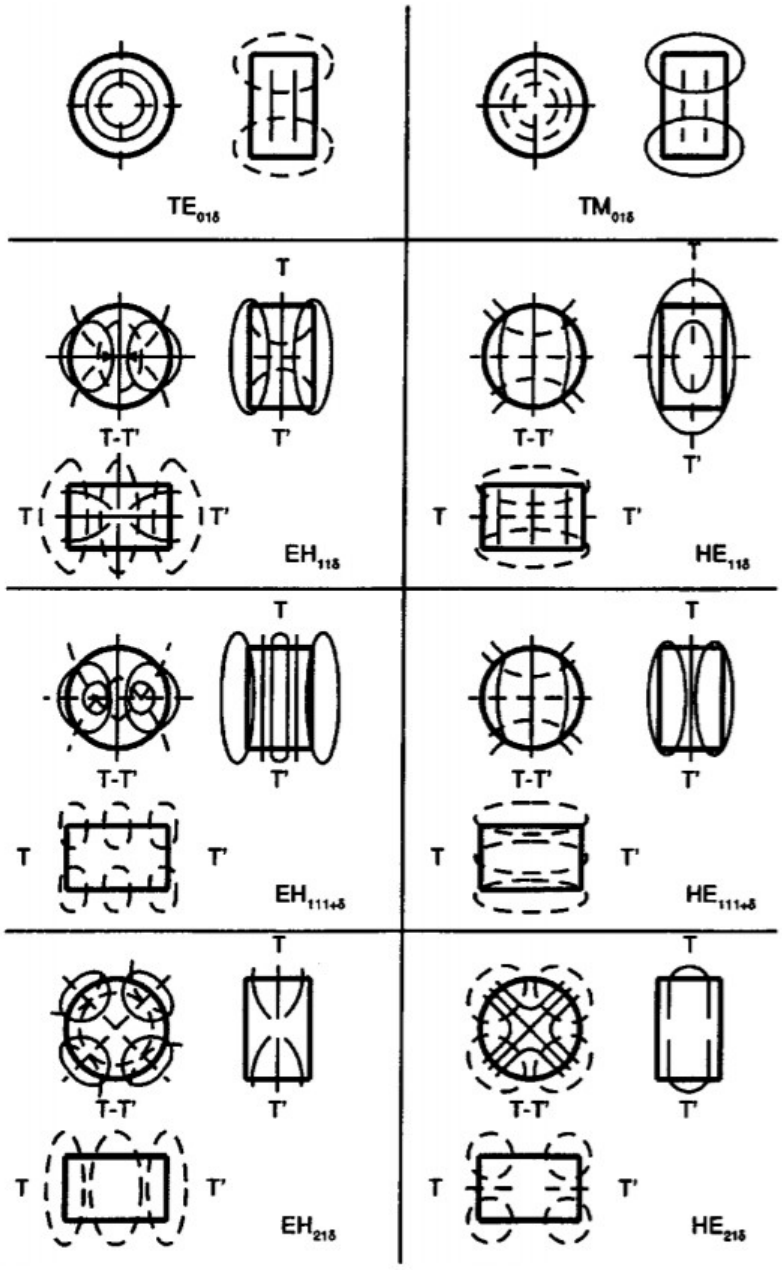

Figure 16: Dielectric resonator modes [19].

Various modes of resonance can be observed in the dielectric resonator. If the dielectric resonator is thought of as a piece of cylindrical waveguide, a transverse electric (TE) mode has no electric field component in the axial direction. A transverse magnetic (TM) has no magnetic field component in the axial direction, usually, z axis. As with rectangular waveguides, there can also exist transverse

electromagnetic modes, which have neither electric nor magnetic field in the direction of the axis.

In contrast with a cylindrical cavity resonator, which is made of electrical conductor and has an ideal boundary condition of E = 0 on its surfaces, the fields of a dielectric resonator are not confined entirely within the resonator. This allows for hybrid electromagnetic (HEM) modes, which can have all six field components, electric and magnetic fields in all three axes. The lowest order mode for a cylindrical dielectric resonator is the TE01 mode [10]. However, hybrid modes can exist at resonances lower than this mode.

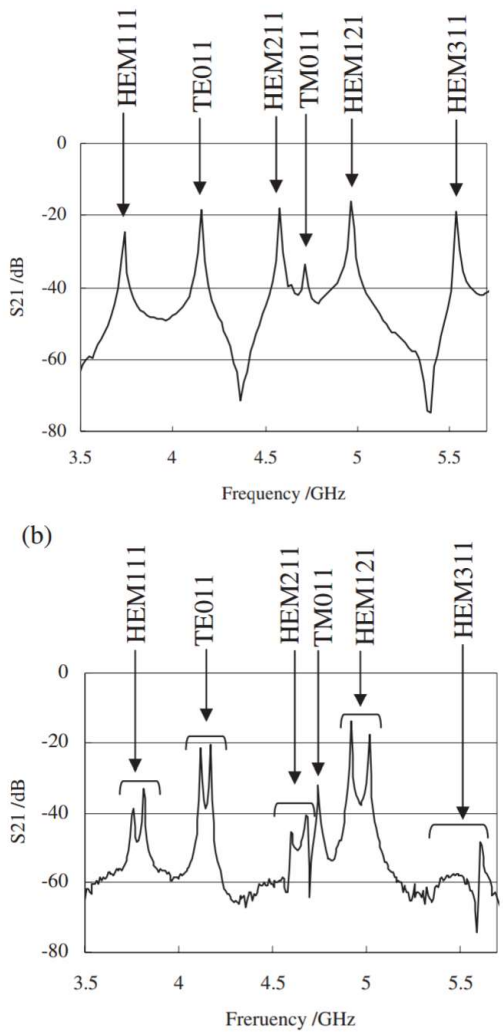

Figure 17: S_{21} transmission plots for (a) single DR and (b) DR pair. Modes are labeled; note how with a pair of resonators, the resonance of each individual DR is shifted either above or below the shared resonance. Resonators are 17.76mm in diameter and 7.88mm in height with a dielectric permittivity of 37.3 [22].

When two identical or near identical resonators are placed with a small separation and excited at microwave frequencies, they couple and a strong electric field can form in the gap between the two resonators. The resonant frequencies for each resonator become "displaced" and shift below and above the original resonance, as can be seen when comparing the left side of Figure 17 to the right side.

Since not all the energy of the electromagnetic fields can be contained in the resonator, there will always be some "spilling" of the electric fields [20]. As mentioned earlier, the Q, or quality factor, relates to the width of the resonance.

However, more generally, and better observed, is this subtle distinction:

$$Q = \omega \frac{\text{maximum energy stored}}{\text{power loss}} \qquad \textit{Equation 31}$$

The earlier definition of Q only took into account the power lost by radiation from the resonator. This second equation more generally accounts for loss not only to radiation, but the material itself. Which accounts for both losses in the material itself (a sort of "friction" that occurs when the polarized molecules react to the electric field) and radiation losses. With this in mind, a more general definition of permittivity should be clarified to take this into account.

We characterize the polarizable property of dielectric material as dielectric loss. Though the permittivity of a material is often thought of as a constant, real valued property, this casually used language refers more specifically to the real part of permittivity. Permittivity is more generally written as a complex valued function dependent on the frequency:

$$\epsilon = \epsilon' - j\epsilon'' = \epsilon_0(1 + \chi_e) \qquad \textit{Equation 32}$$

Where χ_e is called the susceptitibility. The real part of this equation, $\epsilon' = \epsilon_r \epsilon_0$, is the dielectric "constant." The imaginary part of the permittivity is frequency dependent and gives rise to the loss tangent.

Dielectric loss is either described with a loss angle δ or loss tangent tan δ. The loss tangent relates the "lossiness" to the "losslessness" of the dielectric material and can be approximated with 1/Q. In the above definitions of Q, Q is defined as being a frequency dependent relationship between the energy stored over the energy lost. Energy can either be radiated out of the resonator or lost in the material itself as the molecules rearrange under the electric field. This former kind of loss is captured with the loss tangent, but the loss tangent does not account for radiation losses.

We know how to capture dielectric losses. If we return to the equation for polarization, the polarization flux $\bar{D} = \epsilon_0 \bar{E} + \bar{P}_e$ is the sum of the electric field and the polarization vector $\bar{P}_e$. In a linear medium, $\bar{P}_e = \epsilon_0 \chi_e \bar{E}$, so $\bar{D} = \epsilon_0(1 + \chi_e)\bar{E} = \epsilon \bar{E}$. And since $\epsilon = \epsilon' - j\epsilon'' = \epsilon_0(1 + \chi_e)$, we can account for the loss of energy to the heating of the dielectric's vibrating dipoles.

For conductive losses, we need Ohm's Law, which says that for a material with conductivity , $\bar{J} = \sigma \bar{E}$. In Maxwell's equations, this current density $\bar{J}$ affects the curl of the magnetic field by the relationship $\nabla \times \bar{H} = j\omega \bar{D} + \bar{J}$. Substituting, we arrive at the conclusion that the losses due to conductivity (σ) can't be distinguished from dielectric damping ($\omega \epsilon''$):

$$\nabla \times \bar{H} = j\omega \bar{D} + \sigma \bar{E} = j\omega \epsilon \bar{E} + \sigma \bar{E}$$
$$= j\omega \ '\bar{E} + (\omega \epsilon'' + \sigma)\bar{E} \qquad \textit{Equation 33}$$
$$= j\omega(\epsilon' - j\epsilon'' - j\frac{\sigma}{\omega})\bar{E}$$

This means that while a perfect dielectric can be measured with just dielectric loss, there will always be additional conductive losses in a real material that are

indistinguishable those dielectric losses. This term is called the total effective conductivity: $\omega\epsilon'' + \sigma$.

Now we can define the loss tangent described earlier in a more specific manner, as the ratio of the real part of the total displacement current to the imaginary part:

$$tan\delta = \frac{\omega\epsilon'' + \sigma}{\omega\epsilon'} \qquad \textit{Equation 34}$$

Which means we can write permittivity in yet another way, which conveniently separates the dielectric "constant" and the material's loss tangent:

$$\epsilon = \epsilon' - j\epsilon'' = \epsilon' - j(1 - jtan\delta) = \epsilon_0\epsilon_r(1 - jtan\delta) \qquad \textit{Equation 35}$$

This expression is particularly useful because the dielectric properties of a material are given as just dielectric constant and loss tangent (sometimes at a specific frequency), with no mention of dielectric or conductive losses.

There is a frequency dependence because electromagnetic wave propagation depends on μ, ϵ, and σ (the conductivity). As mentioned in Chapter 2.1, the index of refraction n depends on the square root of the product of permittivity and permeability. This is because the previously mentioned phase velocity (or wave velocity), $v_p = \omega/k$, which means that the index of refraction rises with frequency, "bending" higher frequencies or shorter wavelengths by a greater amount. The group velocity $v_g = d\omega/dk$ describes how much each frequency will move when compared to other frequencies.

Even though the index of refraction rises with frequency, near resonance, the index of refraction drops suddenly [6].

Calcium titanate ($CaTiO_3$) is a dielectric material with a high relative permittivity, recorded as 167.7 at lower microwave frequencies and 165 at 3 GHz at room temperature (25 °C). The loss tangents for these frequencies are 2×10^{-4} at lower frequencies, 5×10^{4} at 0.3 GHz, and 23×10^{4} at 3 GHz [23] [24]. 2015, Luo et al. proposed that its high permittivity and low loss would be suitable as an element in a metamaterial. Typically, the electric field is contained within the resonators, especially at such a high relative permittivity, but the resonators can couple when in close proximity and produce a stronger field [25].

CaTiO3 was identified as an attractive element for an all dielectric metamaterial in 2015 by Luo et al. The CaTiO3 resonators used in this thesis had a low loss tangent $\delta\sim5\times10^{-4}$, which yields a quality factor exceeding 1800 for the DR. Sintering a dielectric resonator for longer periods of time may be a way to increase quality factor, since grain size increases [26].

Ceramics made from $CaTiO_3$ have a relatively high temperature coefficient near resonant frequencies, which makes their resonance susceptible to changes in temperature. This makes $CaTiO_3$ an attractive material for thermistors [27], but may present problems with tuning and securing consistent results. It is possible to combine $CaTiO_3$ with dielectric material with lower permittivities but also lower temperature coefficients, sacrificing overall permittivity for greater temperature stability [28].

2.4 Plasma reconfigurable metamaterials

Now that I have covered basic principles of metamaterials and introduced microplasmas and dielectric resonators, I will explain the motivation for combining the latter two to create a reconfigurable metamaterial and why reconfigurability is desirable.

To reiterate, metamaterials are built by combining two kinds of resonant material, and a specific example was discussed where both resonators were made of conductors (split ring resonators and thin wires). It is possible to replace one of the conductors, with plasma, and in fact start plasma with the other resonator type. This thesis begins the investigation of replacing the split ring resonators with dielectric resonators for plasma ignition. If successful, the result is a conductor-less composite medium that might be able to achieve metamaterial properties without interference from wires, electrodes, or other conductors. This new kind of metamaterial could be controlled with the plasma.

One review of reconfigurable metamaterials defines a tunable metamaterial as, "a structure whose electromagnetic behavior is intentionally modified as part of the ordinary operation of the device through… a change in… the unit cell effective circuit, constituent material properties, or geometry" [29]. In practice, reconfigurability means we can control the behavior of the metamaterial, using it either as a switch or some other electrical device [30]. Examples of possible controllable behaviors are changing the permittivity of an antenna substrate or modifying the focal length of a dielectric lens in "real time" [31].

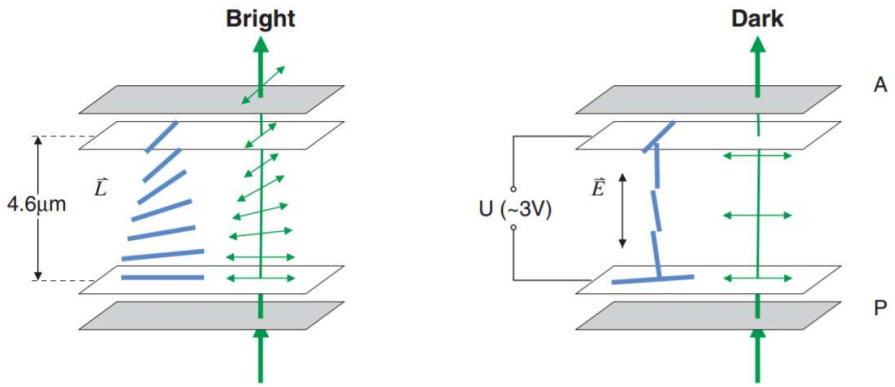

Figure 18: Reconfiguring a liquid crystal: the application of an electric field changes the physical orientation of the crystal, reconfiguring how the light passes through [32].

A liquid crystal is an example of a reconfigurable material. Liquid crystals operate in an optical range. Colors are obtained by optically filtering out the desired wavelength from an external white light source. This is due to the voltage causing the elements of the "crystal" to twist to align in a certain way. At this stage of metamaterial research, there is understanding of how to design metamaterials like crystals – but we are searching for new ways to achieve the "liquid" part of the liquid crystal that allows us to change the properties [32].

Metamaterials must be designed to work with a certain frequency range. This is not surprising since they are built from resonating material that has a relatively high Q, as described in Chapter 2.3. Typically, they are also always "on," that is, once they are built, their properties are fixed and they will always respond in a consistent way. Since many metamaterials are repeating resonant structures, to tune them to a different frequency or introduce any other properties would require changing each sub-element or physically deforming the construction. Due to their construction and repeated structures, most metamaterials cannot be reconfigured for multiple applications or "tuned" in any way.

If designed with this challenge of controllability in mind, metamaterials can also be reconfigured by changing the physical layout of the metamaterial's elements. This method, which is more mechanical in nature, by necessity not only needs considerations such as target frequency, dimensions, fabrication, but also tuning mechanism, what property will be changed, and so on [31]. Though mechanically adjusting a metamaterial with actuators, for example, could work at a larger scale, below a certain dimension, electric control circuits will probably be necessary. This could manifest as a MEMS-based switch, a varactor diode to control capacitance, or PIN diode. Using these elements embedded into the metamaterial would introduce a new set of design parameters including additional frequency responses, extra power consumption, and radiation losses.

Due to their unusual refractive properties, a cloaking surface could be developed with metamaterials. The classic metamaterial construction is copper split ring resonators with thin wires of reflective conductive material. Metal reflects over all frequencies. If we could instead use dielectric material, which is transparent to microwaves, we could achieve greater transparency over a wide frequency band. It also will be convenient to remove conductive elements for other reasons, such as not needing to run wires to the metamaterial, etc. to start the plasma.

Reconfigurable metamaterials can be broadly categorized into several categories based on "intent": tunable filters or antennas, scattering parameter tuners (see Chapter 2.3 for more on S-parameters), spatial tuners (as with a cloaking device or tunable dielectric substrate), and antenna propagation tuners [29].

Since plasmas have already been proposed and used as a common element of metamaterials, due to their negative permittivity below their plasma frequency, some reconfigurable metamaterials have been designed with plasmas [33] [34] [35] [36]. Changing the power and frequency delivered to a plasma can change the electron density and permittivity of the plasma. Thus, it follows logically that the plasma itself can be the element of the metamaterial that allows it to be "tuned" or "reconfigured." However, this is a new enough of an idea that a book published in 2015 (less than two years before this was written, and contemporary to the research conducted) has no mention of "breakdown," "plasma," or "discharge" except in the context of plasma frequency [37].

However, with the addition of microplasmas, it is possible to have a metamaterial that can react to multiple frequencies [4]. In addition, the presence of a plasma can change the frequency response of a structure, with breakdown causing a band stop (opaque) characteristic to disappear (making the structure "transparent") [38].

The metamaterial developed by Singh et al. and shown in Figure 10 has a certain reconfigurability due to its dual-frequency operation. The metamaterial can start plasma at either of two frequencies in the gaps of alternating split ring resonators. It may be undesirable to have the all metal split-ring resonators [16]. This thesis was concerned with developing a metamaterial that could be reconfigured without the need for conductive elements such as wires, electrodes, and plates.

The goal of this research was to create a metamaterial that can be controlled when the plasma is present.

2.5 Related work

At time of writing, there wasn't an experimental example of a reconfigurable metamaterial made from both dielectric material and microplasma, but here I will review some all-dielectric resonators, some plasma metamaterials, and some published work that points in the direction of achieving an all-dielectric plasma reconfigurable metamaterial.

All-dielectric metamaterials seem to be common in antenna or propagation applications. Kamada *et al*. used dielectric resonators in a metamaterial lens antenna to achieve wide angle beam scanning [39]. Li *et al.* propose and prototype a so-called "frequency selective" (or bandpass or bandstop filter) surface by using high-permittivity all-dielectric metamaterial construction [40] Wang *et al.* presented an all-dielectric left-handed metamaterial that did not use or ignite plasma but that also requires the use of a conductive waveguide [41]. Lepetit *et al.* demonstrated that an all-dielectric metamaterial structure can have broadband negative magnetism, a crucial step for creating a plasma-and-dielectric metamaterial [42].

There are some examples of plasma started with dielectric elements, such as in 2002, Remillard *et al.* used a cylindrical dielectric rod and a metal electrode to ignite a plasma and study the dielectric breakdown electric fields in nitrogen. This study involved a dielectric resonator and a metal electrode. The dielectric resonator substituted for one of the "electrodes" to generate plasma with the intent of measuring breakdown of gases [43]. Dielectric breakdown is not by itself a novel

concept, and is often undesirable. But in this thesis, the goal is to generate plasma without metal electrodes.

There are now many more examples of reconfigurable metamaterials. Some of them are mentioned in Chapter 2.4. For example, Zarghooni *et al.* demonstrated a reconfigurable metamaterial used as a dipole antenna. They achieve reconfigurability by embedding three diodes into a double split ring resonator cell [44]. However, there is not yet much literature on plasma reconfigurable metamaterials.

As mentioned previously, Singh *et al.* used an array of split ring resonators to start plasma [4]. In 2016, Cohick *et al.* researched split-post dielectric resonator plasma generators. That is, rather than coupling two resonators together, a single resonator is split in half and the plasma forms in the gap. This research explored $TE_{01\delta}$ and $HEM_{12\delta}$ modes [45]. Kourtzanidis *et al.* proposes submerging an SRR structure into a slab of plasma, and can tune their material by changing the plasma's electron density and collision frequency. They can shift the bandgap using these parameters. The big difference is that their metamaterial does not generate the plasma itself [46]. Sakai and Tachibana claims to have a plasma metamaterial with the permeability changing with input power, [34] [47] taking advantage of the nonlinearities offered by plasma to the metamaterial [48], or generating plasma with slow microwaves in a metasurface [49].

Metamaterials remain the top contender for a cloaking or invisibility device, particularly when active or nonlinear [50] [48]. One method of achieving cloaking is by mapping a transformation to "bend" light around an object [51], but another

method would be impedance matching with free space, as briefly mentioned at the end of Chapter 2.1.

3. Experiments

All of the experiments conducted were fundamentally similar: An antenna transmitted power towards some number of dielectric resonators in a fixed configuration, and the reflection was recorded. This setup not only allows for gathering data but also generating plasma.

Proper atmospheric conditions and sufficient power delivery are necessary for plasma generation. This chapter describes how I generated vacuum and microwave power, measured the systems, and configured the resonators. The fundamental experiment is introduced. In order to achieve breakdown, I needed to control and monitor pressure, system power, and resonator separation.

3.1 Equipment and configurations

3.1.1 Vacuum generation and measurement

This first section describes how to control and monitor pressure in a vacuum chamber.

A vacuum chamber refers to any sealed volume where the gas has been evacuated and the pressure inside is less than atmospheric pressure (1 atm, ~760 Torr, etc.). These conditions are achieved with a mechanical pump in these experiments. An ideal vacuum cannot be realistically reached where no matter is present. In particular, water vapor collects on surfaces and evaporates at low pressure. This means that it is difficult to obtain practical vacuums, and still more difficult to obtain a constant pressure simply by removing the gas in a volume and sealing the chamber. Any leaks will also prove to be a problem.

Fortunately, for these experiments, an ideal vacuum is not needed. Maintaining a relatively low pressure, usually between 1 and 10 Torr, is of more importance. This is a "rough" vacuum, close to the regime between 1 Torr and 10^{-3} Torr [52].

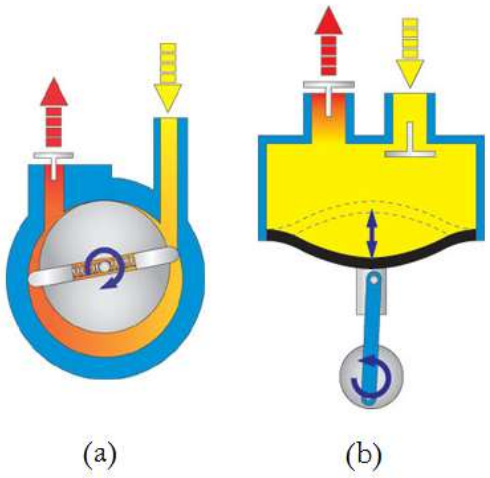

Figure 19: Rough vacuum pumps: (a) rotary valve pump and (b) diaphragm pump [52].

To achieve rough vacuum, a continuous flow is used, and either an oil-sealed rotary vane pump or diaphragm pump is sufficient, shown in Figure 19. Rotary valve pumps work by rotating an eccentrically offset cylinder inside a larger cylinder. There is a valve attached to the inner cylinder that compresses the gas that enters and forces it towards the exit. A diaphragm pump rapidly moves a diaphragm to change the pressure inside the cavity. Two spring loaded valves open in sequence as the pressure level in the cavity shifts from that of the atmospheric pressure. Neither of these options are high quality choices, but as mentioned before, are sufficient for these experiments.

One solution to achieve constant low pressure is to pump a gas back into the chamber while the outside pump vacates the chamber's contents. This has several advantages. The first is that maintaining a constant flow allows for control over the

pressure in the chamber. This is useful particularly if the gas chamber is leaky, because the constant flow can provide a stable pressure. If a stable pressure is set, atmospheric gases will leak in and water will evaporate, increasing the pressure as time passes.

Evacuating a vacuum chamber allows the experimenter to control which gas and how much of it is put back into the chamber. Conventionally, a neutral gas such as helium or argon is used for plasma generation. These experiments utilized argon gas, identified by the purple glow of its discharges. Argon is the cheapest of the noble gases, but also has a low first ionization energy needed to ionize its atoms when compared to gases like helium [53].

If a flow is not used, then the chamber must be pumped down below the desired pressure and then filled back up with the desired gas. Then, this gas is also pumped down to reduce the percentage of leftover contaminant, by the law of proportions. However, the chamber is being continually evacuated with a flow, and the chamber only needs to be pumped down to the proper pressure and not below.

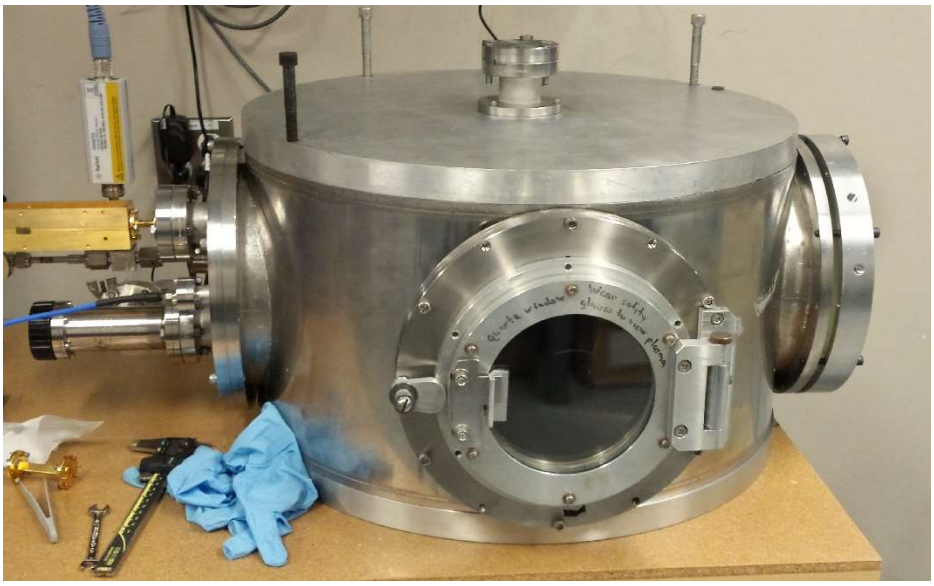

Figure 20: Example of laboratory vacuum chamber.

If a chamber initially filled with atmospheric gas is pumped down to a tenth of the pressure and then "back-filled" up to atmospheric pressure with a pure gas such as argon, it is now 10% contaminated. If this process is repeated and evacuated to a tenth of atmospheric pressure, the chamber will still be composed of argon and the contaminated atmospheric gas, but it will have only 1% of the original atmospheric gas remaining. This is a much faster way to achieve high gas purity at lower pressures than simply turning on a vacuum pump and waiting for it reach low pressures.

The vacuum chamber was 50 cm in diameter by 25 cm high stainless steel, with flanges available for interaction with the outside environment, and is shown Figure 20. These attachments could be electrodes or equipment to start or perform the experiments, sensors or probes to monitor the experiment and collect data, or windows made of plastic, quartz, or glass to view the inside of the chamber and let

photons in. The resonators receive excitation from an antenna through a 19 cm diameter glass window.

Pressure was measured using a piezo-electric pressure transducer for pressures greater than 2 Torr and a capacitive manometer for pressures less than 10 Torr [54]. Piezo electric transducers are semiconductors that take advantage of the piezoresistive effect, the results of mechanical strain changing the electrical resistance of the material. As the gas molecules bounce up against the barrier, the resistance changes [55]. Capacitive manometers use an electrode in reference to a diaphragm that has basically been "tuned" to an absolute pressure. As the pressure deflects the electrode, the capacitance between the electrode and diaphragm changes.

3.1.2 Microwave generation and measurement

There must be a setup to measure how much power is leaving the system and how much is being backscattered or reflected back to the antenna.

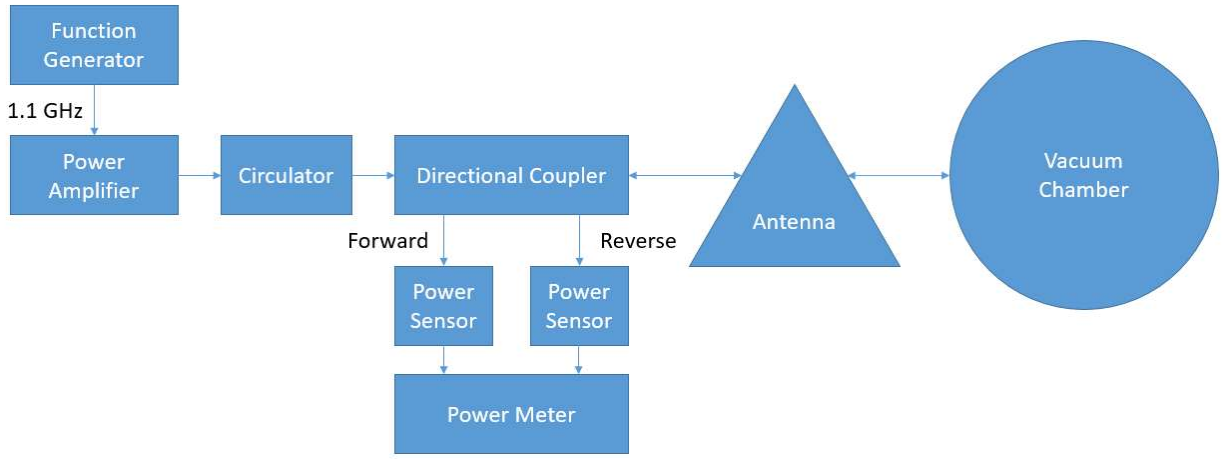

Figure 21: Signal flow for microwave generation and measurement.

The signal flow of my experiments is shown in system form in Figure 21. The desired frequency or frequency range is provided by the Agilent N5183A MXG Analog Signal Generator 100 kHz – 20 GHz signal generator. This signal is amplified to give as high a transmit power as possible by the AR 30S1G4 0.8 – 4.2 GHz 30W amplifier. Then, the amplified signal is fed into a Narda BiDirectional Coaxial Coupler 3022 1 – 4 GHz directional coupler, which has forward and reflected outputs. These outputs are fed into power sensors, which are read and displayed by Agilent E4417A EPM-P Series Power Meter. The direct output from the directional coupler is fed into the antenna. The antenna, shown in Figure 22, transmits into the vacuum chamber through a window (quartz or glass, sometimes with plastic shield) [56].

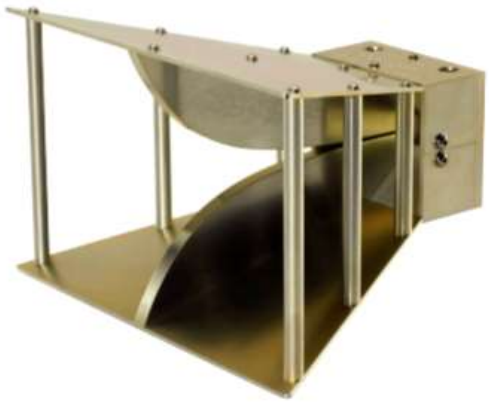

Figure 22: Com-Power AH-118 Double Ridged Horn Antenna, 1 - 18 GHz [56].

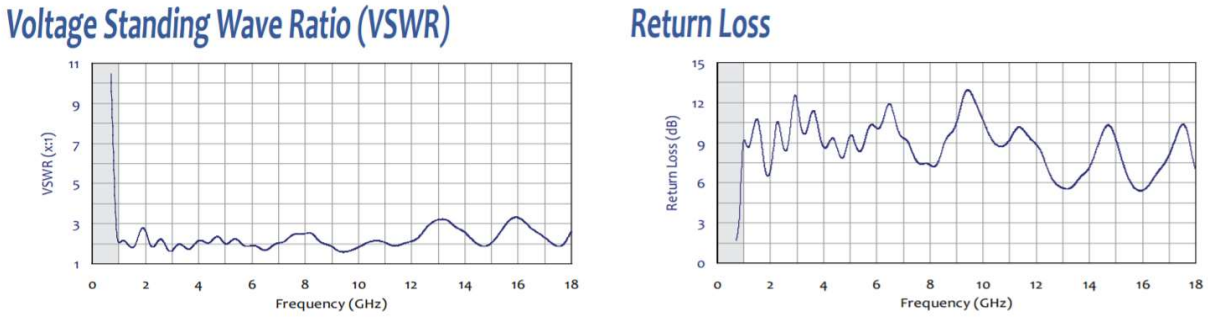

Figure 23: Transmission plots of Com-Power Antenna showing VSWR and return loss [56].

There were some problems with ensuring the proper power. Especially at high frequencies, there are considerable dB losses at each stage and in the cables. This necessitates cables that are as short and lossless as possible to ensure efficient delivery of power to the resonators inside the chamber [57]. We can also only measure the power when it leaves the antenna and not when it reaches the resonator. The wave radiates from the end of the antenna (at the biggest opening of the cone) and must pass through the quartz window and some space before reaching the resonators.

In addition, the frequency responses of the amplifier and antenna were not flat over our frequency ranges. This meant that calibration curves were necessary for taking measurements.

3.1.3 Configurations of resonators

Calcium titanate ($CaTiO_3$) was milled, pressed, and sintered into cylinders with diameters of 28.55 +/- 0.069 mm and heights of 14.724 +/- 0.0764 mm by Penn State University. More measurements are summarized in Table 1. This material was chosen because the dielectric constant is very high (172.47 +/- 0.900) and the loss tangent is low ($\sim 5 \times 10^{-4}$). This gives a quality factor of greater than 1800. The large discontinuity between the ceramic and air results in behavior that resembles a cylindrical cavity resonator. However, as mentioned earlier, there can be fields present outside of the resonator, and these “leaks” from two or more resonators can be paired together.

$CaTiO_3$	
Diameter	30.301 mm
Height	15.219 mm
Weight	42.975 grams
HEM_{011} Mode Resonant Frequency	1.073 GHz
ε_r	164.983
Q	914
Tan δ	1.094×10^{-3}

Table 1: Sample properties of calcium titanate ($CaTiO_3$) as measured by PSU with the Hakki-Coleman [58] method.

Figure 24: Teflon (PTFE) stand for one dimensional array.

A stand was built of Teflon to hold the resonators in place. Teflon was chosen because its relatively low permittivity ($\epsilon_r \sim 2$) gives it a strong enough contrast with the $CaTiO_3$ ($\epsilon_r \sim 170$) that it does not interfere. Designed with a vice or clamp in mind, there was a base made from ½ inch thick by 5" by 2" Teflon blocks, four ½" diameter partially threaded rods screwed in each corner, and ¾" by ¾" by 3/8" nuts to hold the blocks in place. The rods were threaded and nuts were made from square sections of the Teflon. The nuts allowed the adjustment of the height between the

two holder platforms and the relative height of the whole assembly. There are two platforms that can be adjusted in relative height. The clamps ensures that once the resonators are positioned, they don't move. The extra Teflon slab seen In Figure 24, attached on the bottom of the stand, provides balance.

The platforms themselves had two channels, one which was as wide as the diameter of the resonators, and another in channel in the middle of the previous channel which was as wide as the height of the resonator. This allowed for the resonators to be oriented in one of two directions. The antenna was either pointed towards the YZ plane (resonator pair) or XZ plane (five resonator array).

The resonators were put in between the holder platforms and the top platform was "clamped" down. A shim or spacer was put in between the two resonators to achieve the proper separation. However, while any spacing could be achieved, it was difficult to ensure a spacing below a tolerance of 1 mm because we did not have shims smaller than 1 mm. The spacers could not be left in the array because there should be free space between resonators.

3.2 Procedures

3.2.1 Measuring properties and modes of resonator materials

Before plasma could start, resonances had to be experimentally located. Doing this would also allow an indirect measurement of the permittivity of the material using the temperature coefficient of the material.

In order to confirm the electromagnetic properties of the dielectric resonator, several tests were performed. The initial goal was to detect resonances in dielectric

resonators. With a network analyzer unavailable, a frequency sweep was performed in time. The signal generator was programmed to sweep a frequency range, and the results were sampled. These are radiated towards the resonator by an antenna. A directional coupler was used to record both incident and reflected power.

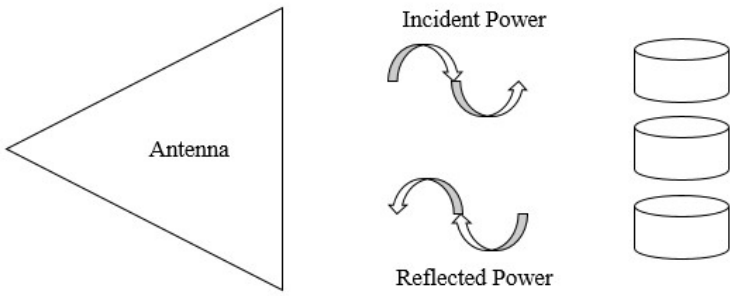

Figure 25: Antenna transmits power to the resonator arrays but also captures reflected power.

The resonance and electrical properties of the resonators had been experimentally measured by Penn State University using the Hakki-Coleman method [58]. This involves clamping the resonators between two "infinite" conductive plates and then probing the electric field across the cylinder. However, the conductive plates prevent any radiation of the dielectrics in the Z-axis, changing the modes present in the resonator [58]. Since the radiation is not bounded in the actual experiments, we had to ensure we were still using the correct dielectric and loss parameters.

The relationship between the forward power of the antenna and the reflected power is one of several scattering parameters, here called S_{11}. S_{11} is formally called the "input port voltage reflection coefficient." The plot of S_{11} demonstrates where a resonance might be. A sharp discontinuity in the S_{11} curve could be the result of an increased absorption or reflection by the resonator. Our method of locating resonances without the conductive plates was to locate discrepancies in reflection

between when the resonators were or were not present. This required evaluating a calibration curve by measuring the environment without the resonator present and comparing that to the data taken with the resonator present. Any reflections or absorptions when removing the calibration data from the data with the resonators present could indicate a resonance.

Figure 26 shows the reflection curve both with and without resonator. The sharp discontinuity which appears when the resonator is present suggests this is the resonance located in simulations, which will be explained in the following Chapter 4.3. Reflection in these plots is simply reflected power divided by incident power.

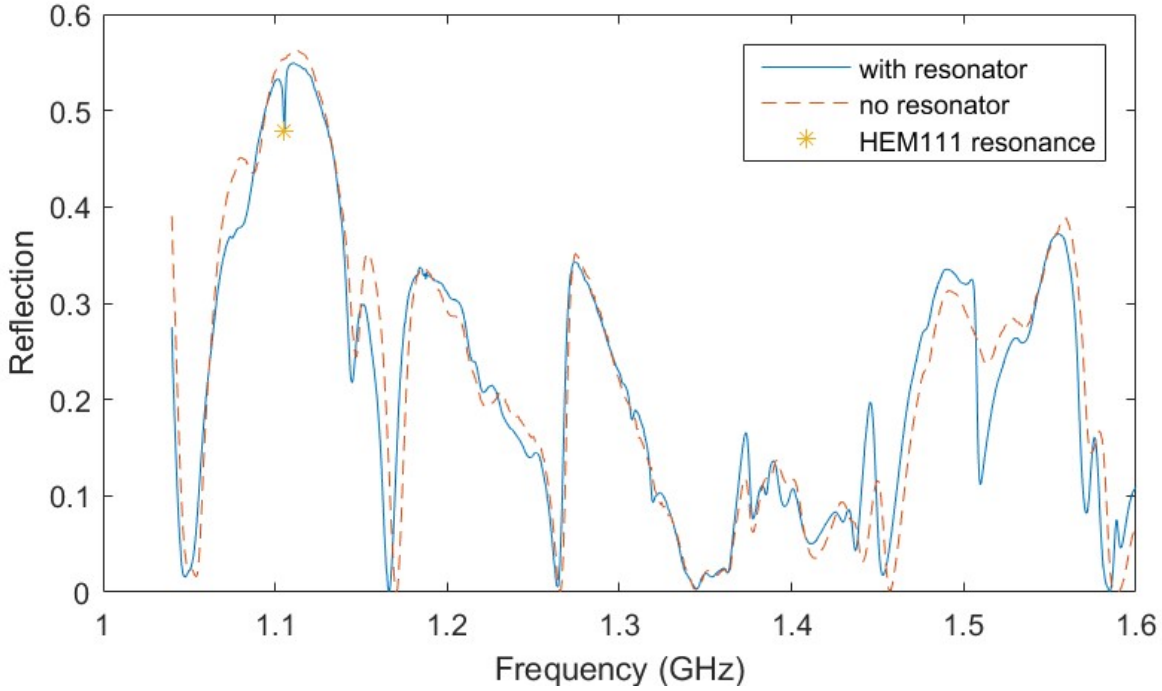

Figure 26: Experimental reflection curve showing location of HEM_{111} resonance. Reflection is reflected power divided by transmitted power.

In the process of sweeping the resonator, we discovered that the resonator was heating up at a rate that was noticeable by the sensitivity of a human hand. Since

the resonant frequency was shifting as well, I wanted to know how much the change in temperature was affecting the permittivity of the material.

The $CaTiO_3$ resonators were heated with a heat gun and allowed to cool to room temperature. As the resonators cooled, the resonance was measured with the S_{11} sweep described above. By tracking how much the resonance changed with temperature, the amount that the dielectric constant changed with temperature could be calculated.

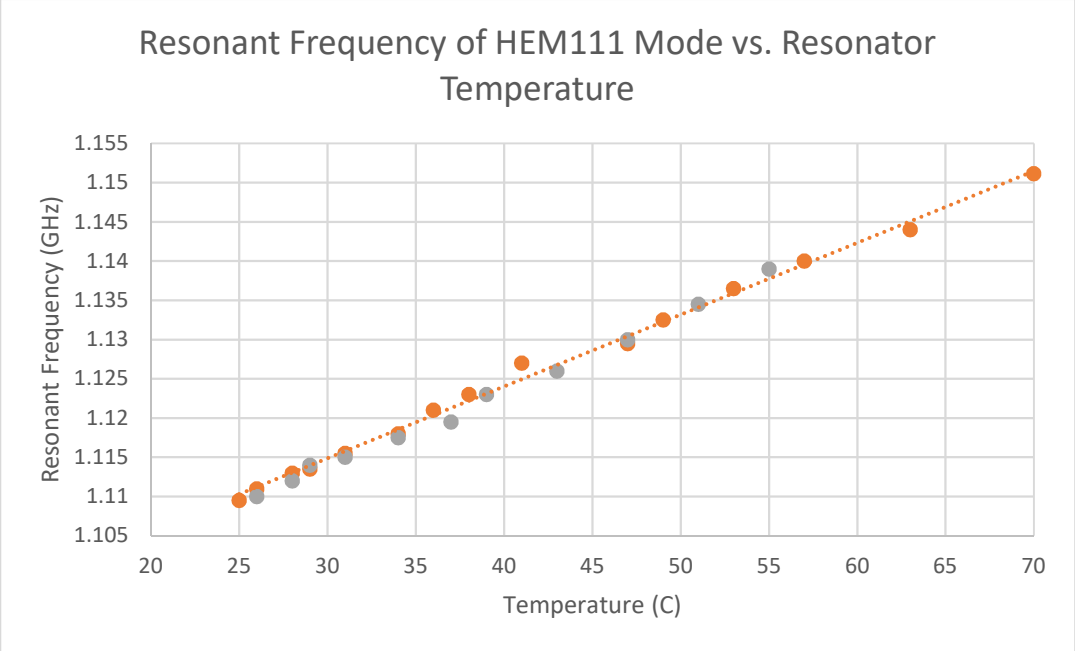

Figure 27: Plot relating resonant frequency and resonator temperature.

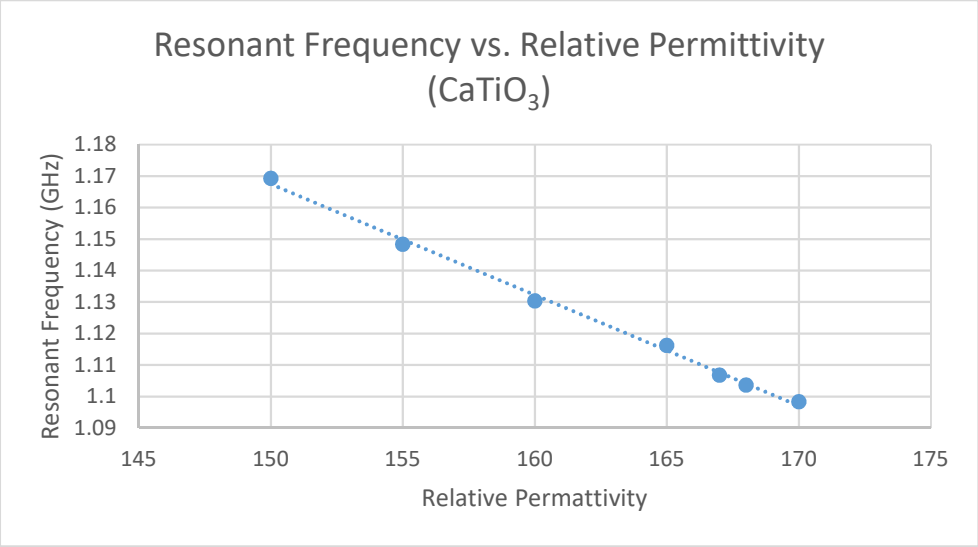

Figure 28: Plot relating resonant frequency and relative permittivity of HFSS model.

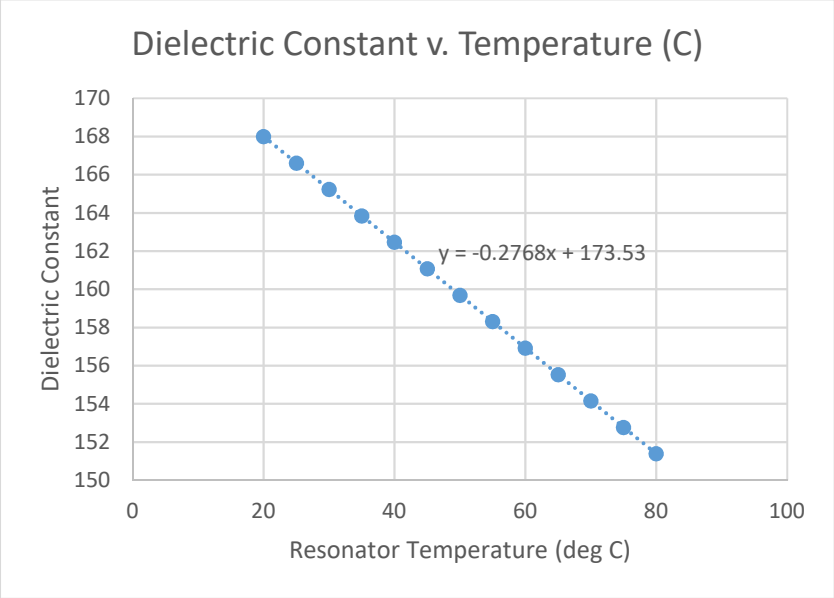

Figure 29: Plot relating dielectric constant and resonator temperature.

Cockbain reports the dielectric of $CaTiO_3$ to be 160, with a loss tangent at 1 MHz of 0.0002 – 0.0008, and a temperature coefficient of permittivity at 20-80 $°C$ of -1600 parts in 10^6/°C [59]. Kell, Greenham, & Olds approximate the temperature coefficient of $CaTiO_3$ as $\frac{d\varepsilon_r}{\varepsilon_r dT} \approx -10\varepsilon_r \left(\frac{ppm}{°C}\right)$. For calcium titanate, with a permittivity of ϵ_r~165, this gives an approximation of $\frac{d\epsilon_r}{\epsilon_r dT} \approx -10(165)\frac{ppm}{°C}$ or,

when denormalized, $\frac{d\epsilon_r}{dT} \approx -10(165)^2 \frac{ppm}{^\circ C} = -0.27225 \frac{units}{^\circ C}$. Each degree shift in temperature results in about a -0.27 shift in the dielectric constant [60].

By relating resonant frequency and temperature to permittivity and temperature, the permittivity of the resonators could be determined at room temperature. The experimental derivation was calculated to find a shift in temperature for each degree to be about -0.2768 units per $^\circ C$. By comparing the sweep to the simulated results, the dielectric constant of the resonators can be confirmed. Since room temperature was measured to be 20 $^\circ C$, the permittivity of the resonators was about 168. One study suggests that loss tangent decreases as temperature increases, which means that as the resonators heat up, their Q decreases [61]. This implies that a 'hot' resonator not only has a different resonant frequency but may produce a lower electric field for starting plasma due to a decreased Q factor. This is a consideration for operating an array of plasma for long periods of time.

3.2.2 Fundamental array experiment

The fundamental experiment in this work was performed with the signal flow described in sections 3.1.1 and 3.1.2. Some resonator configuration was put into the vacuum chamber, and then the vacuum chamber was evacuated to a low pressure. The basic idea was to light the plasma and take some measurements.

Lighting the plasma involved starting at a frequency below the known resonance and slowly increasing the signal generator's frequency until the plasma lit. In order for breakdown to occur, as mentioned in Chapter 2.2, there must be sufficient breakdown voltage on the order of $10^5\ V/m$. Simulations described in Chapter 4 suggested that one resonator could resonate with an electric field as strong as

$10^4\ V/m$, which is an order of magnitude too low. When that resonator is coupled with an identical resonator, the electric field in the gap between the two resonators can increase by an order of magnitude. In addition, the fields of a single resonator are confined mostly within the resonator; coupling two resonators creates a strong electric field in the free space gap between the two resonators.

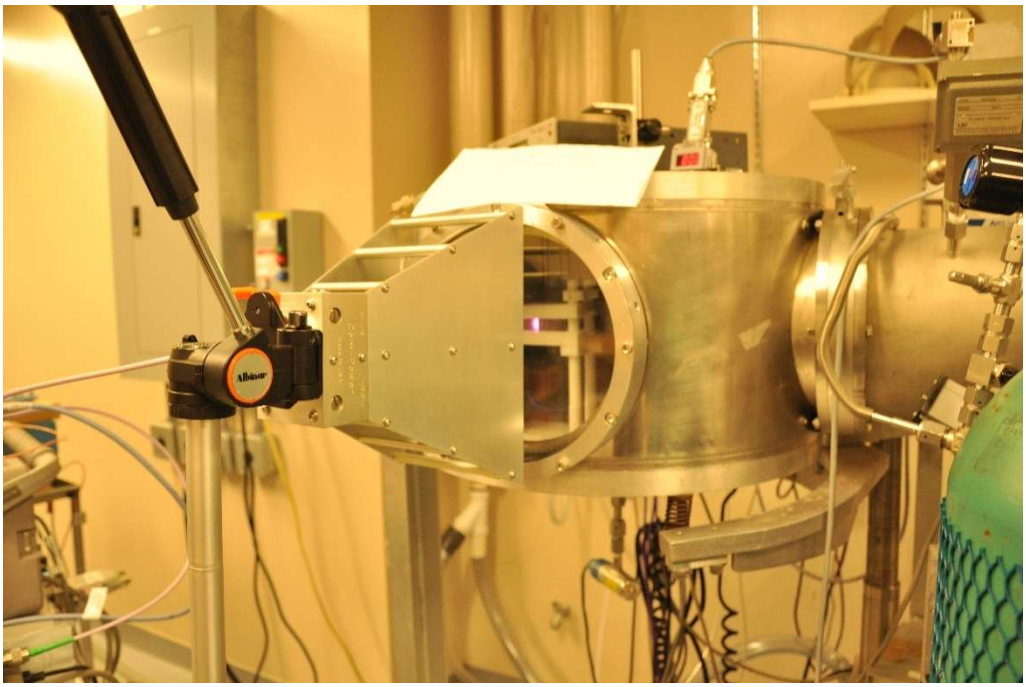

Figure 30: Horn antenna with antenna against glass window with ignited plasma (purple) visible in Teflon stand.

First the goal was to start plasma with a single dielectric resonator with the help of a high voltage probe. Then a pair of resonators were used to start the plasma with the intention of advancing from a point (between two resonators) to a surface (five by five resonators) to a volume (5x5x5 resonators). The experimental setup was a vacuum chamber pumped down below 1 Torr and then backfilled with argon. The resonator setups were supported by a Teflon platform.

Starting a plasma with just one resonator required using a high voltage DC source, essentially a sparkplug lighter, in the vacuum chamber. A plasma was lit using the exposed wire (coax with the outside conductor removed) at a forward power of 24W. When microwave signal at the resonance of the dielectric resonator was applied, a plasma lit around the dielectric resonator. It was sustained by the microwave power when the DC voltage was removed. This demonstrated that while a single resonator could not ignite a plasma, it had sufficient resonance to sustain the plasma with just microwaves. However, one resonator did not have the necessary field strength to start a plasma on its own. It was also clear that more energy was needed to initiate breakdown than to sustain a plasma.

The resonators increased in temperature when the plasma was ignited, so the permittivity and dielectric constant drifted as experiments were run. This required occasionally locating the resonant frequency and is not at odds with studies of other plasma-generating resonators [17].

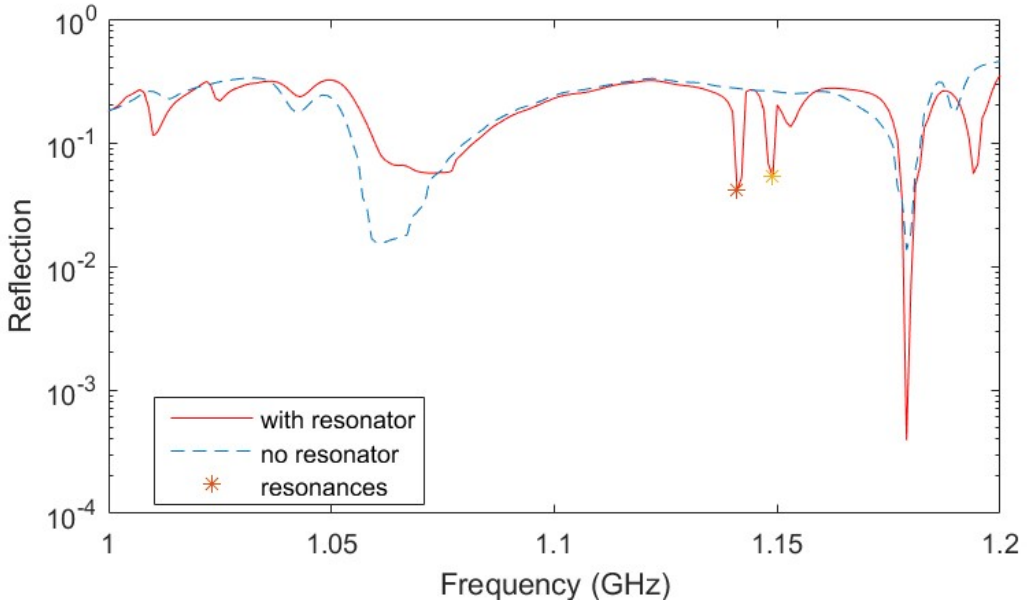

Figure 31: Reflection curve for resonator pair, note the shifts both above and below the resonant frequency located in

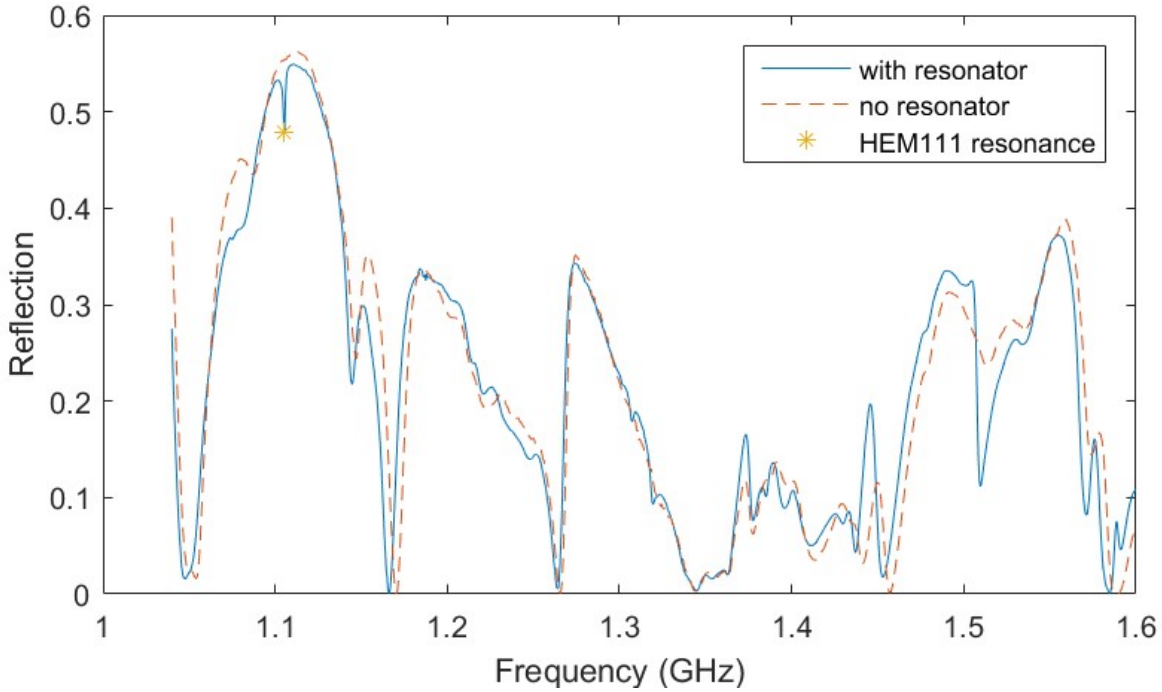

Figure 26.

The next step was to couple two identical resonators with diameters of about 28.5 mm and heights of 14.7 mm together and systematically vary the separation between the two. The separations chosen were 0.5 mm, 1 mm, 2 mm, 3 mm, 4 mm,

and 5 mm. Two resonators have a strong enough electric field in their gap to start a plasma without the need of an auxiliary source. While the resonators had similar dimensions, none of the resonators used were identical due to the manual fabrication process. Three or more resonators could be lit by lighting the matched pair then changing the frequency of the signal generator to match the resonance of the remaining resonator. Once the plasma was lit, the pressure was increased to atmospheric pressure (~760 Torr) by adding more argon. The plasma remained lit at atmospheric pressure and changed color from violet to a more brilliant white.

Figure 32: Orientation of resonators in reference to antenna. Note direction of E field. The resonator pair and five-element array are oriented in different directions.

As mentioned in Chapter 3.2.1, because the resonator increased in temperature during each run, during subsequent trials the ignition frequency increased as well. There was no visible damage to the surface of the dielectric resonators following these experiments.

The resonator pair was used to light plasma at various pressures and separations. This data, along with the forward and reflected power, was used to create a plot and find the minimum power required for breakdown at each P*d (pressure times distance). The separation *d* is the minimum gap between the volumes of the resonators, since the resonators are curved. This means that, unlike the parallel plate

electrodes described above, which have a constant separation, there is no unique or distinct place for breakdown to occur between the resonators.

4. Simulations

The experiment described in Chapter 3.2.2 was modeled and simulated before it was implemented in the lab. As the experimental procedure was refined, so was the experimental geometry of the simulation improved. These simulations were developed and executed with Adam Chapman.

4.1 Ansys HFSS

Ansys (Ansoft) High Frequency Structural Simulator (HFSS) was used for simulations. HFSS utilizes the finite element method of numerical analysis to solve Maxwell's equations and determine the fields and waves inside of the resonators.

HFSS breaks the structures inside of its simulation into a discretized mesh. This mesh is made of triangular pyramids, and Maxwell's equations are solved inside of the mesh. In general, the finer the mesh, the less approximate the solution will be.

These partial differential equations are solved not just for one set of conditions at one frequency, but over a broad sweep of frequencies. When the scattering parameters are plotted over the curves, resonances can be detected. They are clear because most of the frequencies, the reflection is higher. However, when a resonance is reached, the resonator absorbs most of the energy, causing a prominent dip in the S_{11} curve, as introduced in Chapter 2. We are looking for either a prominent dip or spike in the reflection, like with the experimental method in Chapter 3.

It is important to note that plasma was not modeled in these simulations and that the gap between resonators was free space. The simulations were used to model the

resonances and modes of the resonators and determine if the electric field was strong enough to achieve breakdown.

The simulations focused on scattering parameter S_{11}, electric and magnetic fields, and power with the goal of finding sufficient electric field for plasma breakdown rather than simulating plasma behavior.

4.2 Models

The Com-Power antenna described in Chapter 3.1.2 was measured and modeled in HFSS. A comparison of the two is shown in Figure 33: Left: 1-18GHz Com-Power AH-118 antenna, Right: HFSS model.Figure 33.

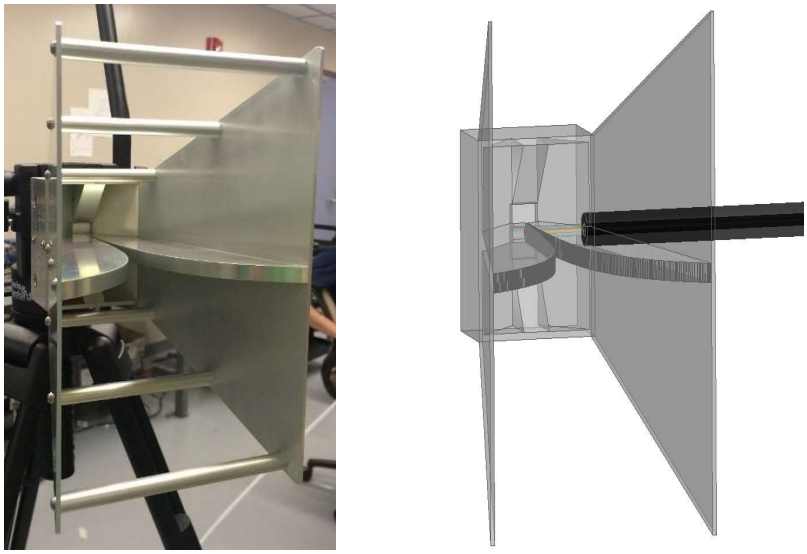

Figure 33: Left: 1-18GHz Com-Power AH-118 antenna, Right: HFSS model.

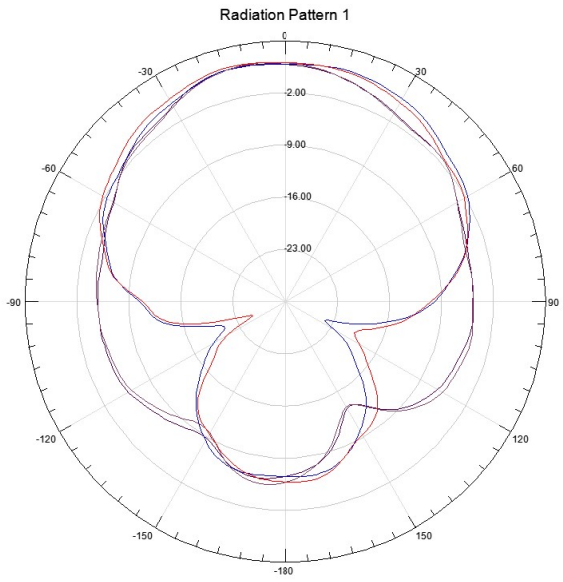

Figure 34: Radiation pattern (gain) of HFSS model of antenna.

The vacuum chamber was modeled by measuring the diameter of the chamber, window, and depth of the flange and window. The chamber was modeled as *PEC* (perfectly electrical conductor) rather than aluminum, ensuring perfect electromagnetic boundary conditions and reducing the computational complexity of the problem.

The antenna was measured and modeled with PEC material in HFSS. This is a convenient, ideal behavior that makes computations faster. As briefly discussed in Chapter 2.3, perfect conductors have no resistance, no internal electric field, and infinite electrical conductivity.

In these simulations, the outer bounds of the simulated volume were selected as perfectly absorbing material, meaning that no radiation hitting the outer boundary was reflected back. Any radiation scattering to the boundaries would disappear as if propagated into infinite free space.

There were two setups used for the breakdown simulations and experiments. One was with a pair of resonators, the second was with a five-resonator array. These match the experimental setups.

4.3 Fundamental simulation

These experiments were all simulated with the same basic setup of the laboratory experiment. At best, the simulation should yield the same results as the experiment. At their lowest resolution, the simulations were used as confirm trends or discover the feasibility of experiments. The simulations either quantitatively aided the data collection process or provided a qualitative demonstration.

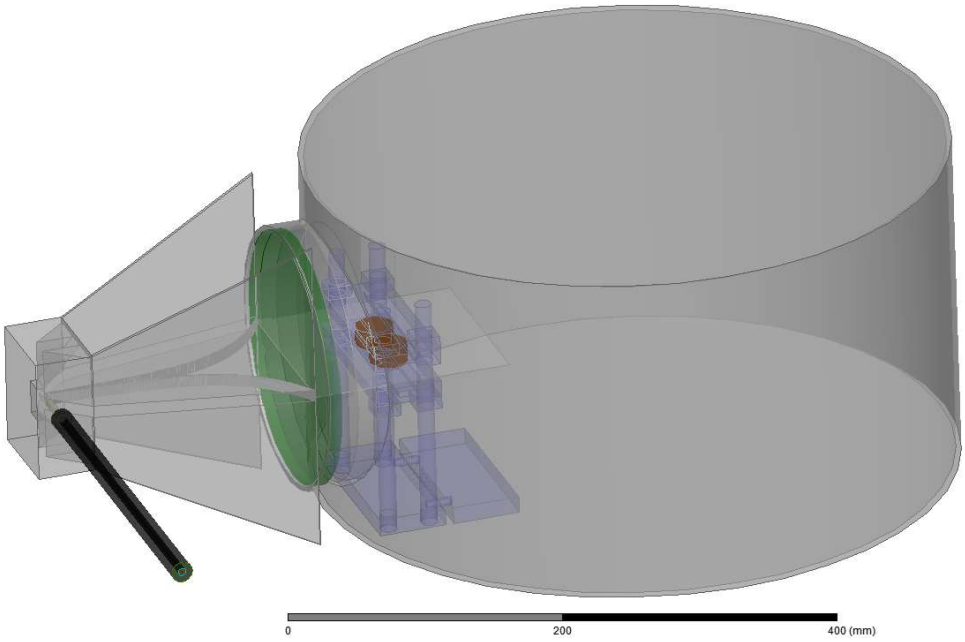

Figure 35: Cross sections of fundamental simulation, with coaxial line leading to the horn antenna, which transmits through the quartz window to the cylindrical dielectric resonators inside (clamped in a Teflon stand).

There is an antenna transmitting into free space with one or more resonators in front of the antenna. The simulation runs a frequency sweep and the S_{11} parameter is plotted with frequency. This plot is compared to a simulation of the vacuum

chamber with no resonators. The S_{11} plots can be compared to the calibration plot to determine if the suspected resonances are due to the presence of the resonators, the model, or the antenna itself.

Typically, I would perform a longer sweep with a low frequency resolution, locate the areas of strong peaks, and then sweep those peaks with a finer resolution. The goal was to find both a strong electric field and a "well-resolved" mode.

HFSS simulation was used to calculate electric field, determine the S_{11} curve (reflection over a given frequency band), and confirm the properties of $CaTiO_3$.

This means that HFSS was used primarily to find the electric and magnetic fields at certain frequencies in a given sweep.

When locating a resonance, the S_{11} curve was computed to find differences in the chamber when resonators were or were not present, equivalent to the experiments from Chapter 3.2. When determining the relationship between permittivity and temperature, simulations were made to connect permittivities to resonant frequencies, which were also tracked with the computed S_{11} curves.

When a suitable mode was identified, the electric field strength at that mode was then measured to determine if breakdown could occur.

The most important features that the simulation needed to accurately model were the dimensions of the electromagnetic features (resonator and antenna), the permittivity of the resonators (and their discrepancies), the distances between the features. The pressure was not taken into account in these experiments since the plasma was not being modeled.

4.4 Locating and identifying modes

As described and defined in Chapter 2.3, the modes of a dielectric resonator are frequencies where the electric field arranges itself inside and outside the resonator.

Since these modes cannot be seen explicitly inside an opaque resonator, and not visually in experiments, their existence is tested experimentally and confirmed in simulation. By plotting the electric field magnitude, the characteristic lobes, nodes, and nulls of resonator modes can be visualized. The steps are to simulate a resonator using the known properties of the dielectric, locate a resonant frequency, then go to the lab and sweep near that frequency. When the resonant frequency is found experimentally, the simulation can be improved by modifying the properties (usually permittivity) and simulating until the simulation matches the experimental results.

The first step was to suspend a resonator in free space and simulate reflection from a patch antenna. This way, the only material in the perfectly absorbing chamber is the resonator, and the resonances can be easily seen. Then, the rather complex antenna model is used rather than the patch antenna, and the resonant frequency is tracked. Finally, the whole simulation with vacuum chamber, window, and stand is used for simulations that require quantified data discussed in Chapter 5.1.

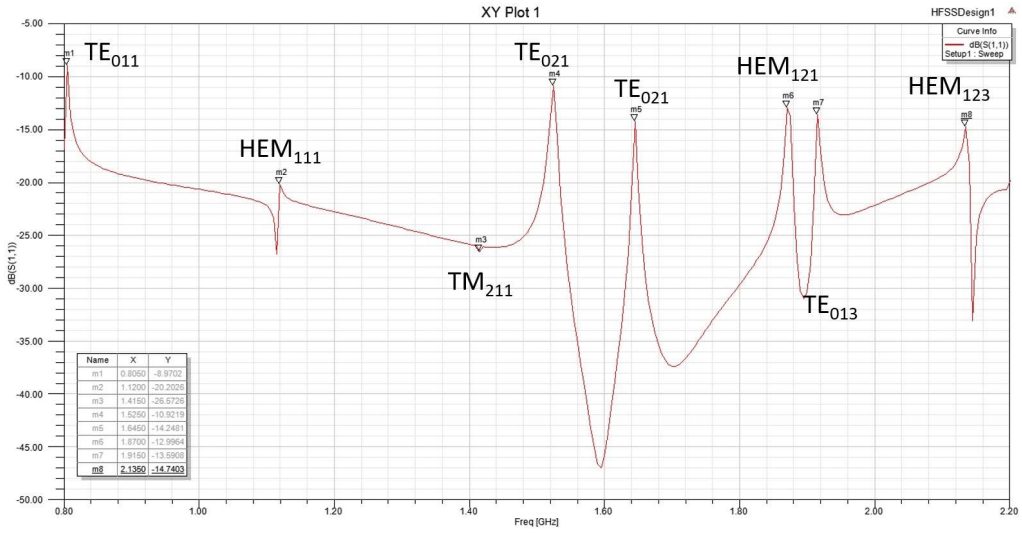

Figure 36: S_{11} plot of single resonator with labeled modes.

Previous research with plasma generation by resonators at low pressure suggested that an electric field in excess of 1 kV/m would be needed for breakdown. Two modes were found for a $CaTiO_3$ resonator that generated a field of about 1 kV/m at 1 W of input power. Figure 37 and Figure 38 show simulated magnitude plots of electric and magnetic fields, respectively, of the HEM_{111} mode in a single resonator.

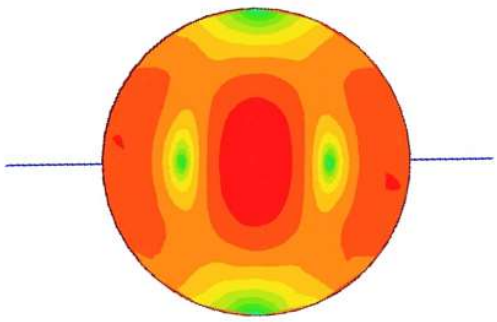

Figure 37: HEM111 mode inside CaTiO3 resonator, E field.

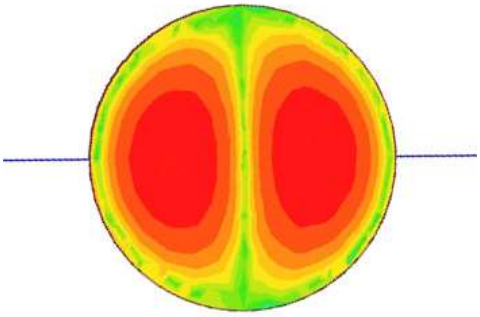

Figure 38: HEM111 mode inside CaTiO3 resonator, H field.

More modes and their associated figures are given in the Appendix.

Figure 39 compares both TE_{011} and HEM_{111} modes in single resonator and resonator pair configurations. The top row of Figure 39 shows these modes and their associated vector fields. While there is a strong field inside the resonators, due to their dielectric nature, there is also strong field "leaking" out of the resonators. Yet, these fields (at 1 W input power) were not strong enough to start a plasma.

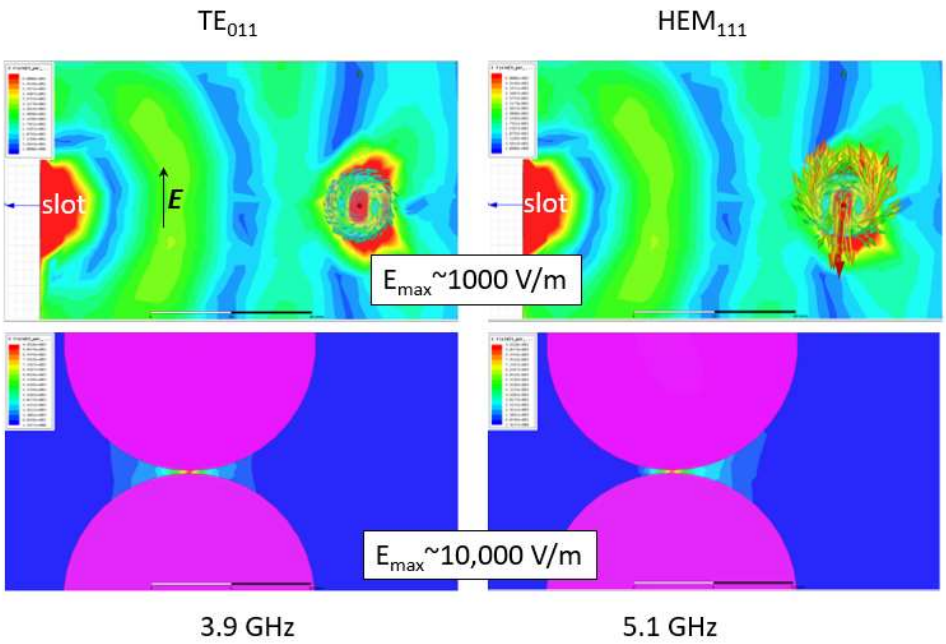

Figure 39: Electric field simulations for TE011 and HEM111 single resonators and pair of resonators (top and bottom rows, respectively) with a 160 μm separation. Note these are resonators of a different size than used in plasma generation.

Two resonators of the same size can couple at the resonant frequency when placed close enough together. When the same resonators used in the top row were doubled, with a gap of 160 μm, electric fields of an order of magnitude stronger were reached. The hybrid mode HEM_{111} was found to have stronger fields than the TE_{011} mode, and so this basic setup (bottom right corner of Figure 39) was used in initial experiments.

5. Results and discussions

This section presents the results of the experiments and simulations. First, I explain how breakdown was achieved and the necessary conditions for breakdown to begin. Then, I discuss how the electromagnetic scattering was reconfigured and its implications for reconfigurable metamaterial structures.

5.1 Breakdown

5.1.1 Method for determining voltage from experimental data

Continuing from the discussion of resonant modes and electric field strength, once a proper resonance was located and sufficient power applied, plasma was ignited. For a pair of resonators, plasma started at 25 W. Once I could start the plasma remotely with microwave power, I wanted to figure out the optimal conditions for breakdown. The plasma could be started with as little as 1.57 W at 1 Torr with a separation of 1 mm. I wanted to find the pressure and separation that required the lowest amount of input power.

The second step was to determine how breakdown voltage changed with pressure and gap size. The forward power leaving the antenna was measured starting at a low power where the plasma had not ignited. The power was increased in small increments until the plasma began. This minimum power required to start plasma can be displayed as a function of pressure times resonator separation (Torr-cm) in the canonical pd form. Figure 40 provides an example of a DC study of parallel plate separation and breakdown voltage.

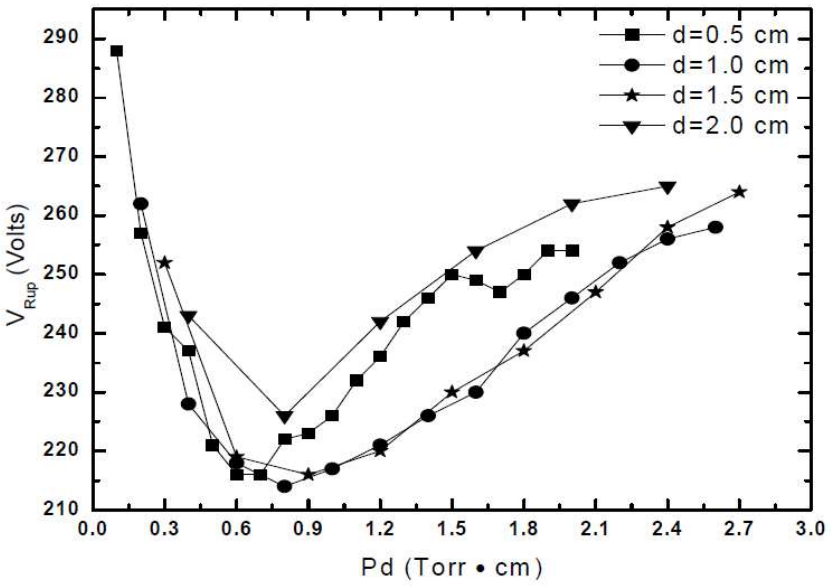

Figure 40: Example of Paschen's curve obtained by varying the Ar gas pressure and distance between copper electrodes [62]

By representing each gap size with its own data series, with gap sizes ranging from 0.5 mm to 5 mm, information is conveyed about gap, forward power, and pressure in one plot. This process is shown in

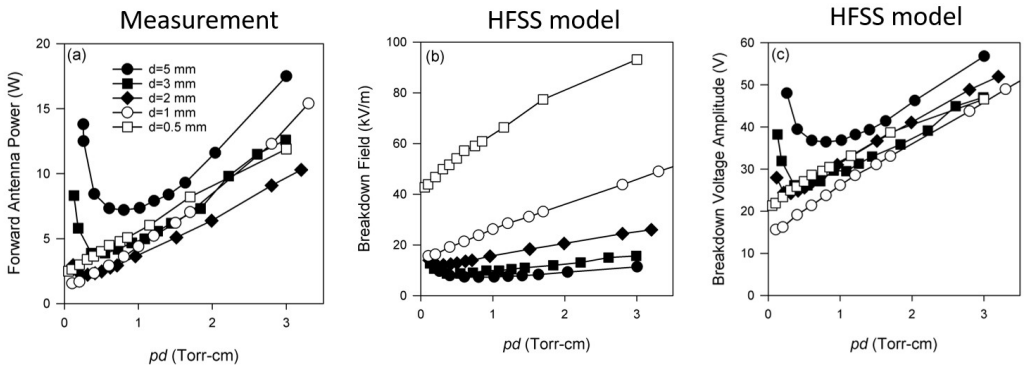

Figure *41*, where the use of Pd becomes more clear: if the same data had been tabulated on an axis for just pressure, data points for a gap of 0.5 mm would have been spread out from 2 Torr to 60 Torr while data points for 5 mm would have been compressed into 0.2 Torr to 6 Torr. The plot generated below is based off of a

conventional Paschen's law curve for DC breakdown in Argon with copper electrodes shown in Figure 40: Example of Paschen's curve obtained by varying the Ar gas pressure and distance between copper electrodes [62].

These forward power measurements were then entered into HFSS simulations with the appropriate gap sizes for each data set. No changes or assumptions were made in pressure. HFSS calculated the electric field between the resonators and the data for the second plot measures the electric field at a point equidistant from both resonators in the gap. This simulation show the instant before breakdown occurs. The presence of the plasma probably changes the actual E field in the gap once it has ignited, but less power is required to sustain than to ignite plasma. Finally, the breakdown voltages were calculated by integrating across the shortest distance between resonators.

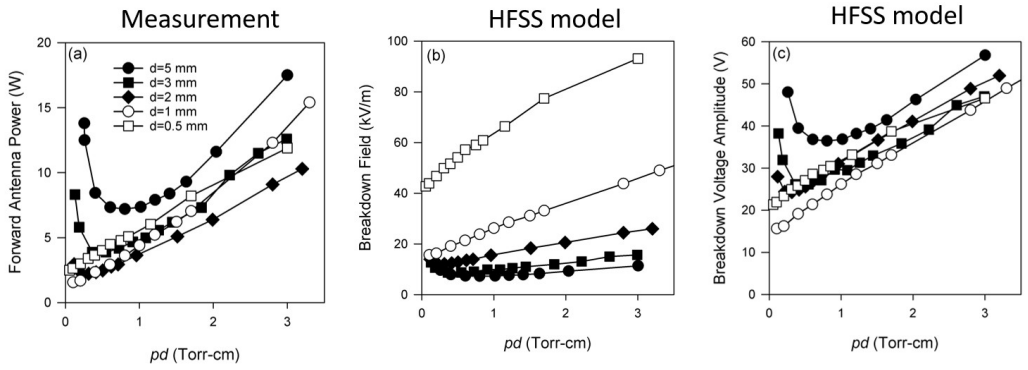

Figure 41*: Combining experimental data and simulations to determine breakdown voltage.*

5.1.2 Results & discussion of breakdown characteristics

For the breakdown experiments, there were two "families" of data curves, distinguished in Figure *41* by the closed shapes (gap separation > 1 mm) and open shapes (gap separation <= 1 mm).

Resonator pairs with separations of greater than 1 mm appeared to follow an argon breakdown Paschen curve-like behavior as shown in Figure 40. In general, all separations had lower breakdown voltages as the pressure decreased, but for separations greater than 1mm there was an inflection point where the breakdown voltage was lowest. At lower pressures than this inflection point, the breakdown voltage was higher.

As the gas particles become less densely packed, there are less collisions to prevent the gas from ionizing. However, the gas reaches a point where it becomes too sparse, and the electrons are accelerated by the electric field without hitting another particle [62] [13].

By contrast, separations of 0.5 mm and 1 mm continued to have lower breakdown voltages as pressure decreased. This means that while gaps of > 1mm had a minimum power between or near 0.3 and 0.8 Torr-cm, there was no minimum power experimentally found for gaps 1 mm and smaller. Paschen curves are not strict laws, and cannot ensure accuracy in high or low pd settings.

It should be noted that because the resonators have curved surfaces, there is no obvious path for breakdown to occur, meaning that this study cannot be directly compared to that of parallel-plate breakdown. It is possible that for gap sizes less than 2 mm, the plasma is "choosing" a larger separation due to the curved surfaces. This seems to correspond more to the breakdown limits in free space than to the confines of the gap [43].

These experiments demonstrated that it was possible to start plasma with the resonator pair at voltages as low as 15 V, and at most 57 V. This corresponds to forward powers (leaving the antenna) as low as 2 W and no higher than 20 W. Since the power is not directed once it leaves the antenna, and must pass through space and a glass boundary, even less power is reaching the resonator array when the plasma begins.

For breakdown in general, I will discuss the five-resonator array briefly. As can be seen in Figure 42: a) Five resonator array, b) Simulated electric field (6.3 kV/m @ 1W), c) Low pressure operation: 0.8 Torr, argon 25 W, d) High pressure operation: 730 Torr, argon 10.5 W ., five resonators ignite four regions of plasma. For the five resonator experiment, since no two resonators were the same size due to the manual fabrication techniques, there was a spread in resonant frequencies. This required igniting plasma on a subset of resonators and then slightly adjusting the excitation frequency to ignite the remainder.

Multiple filaments were visible from resonator to resonator, and when the pressure in the chamber was raised to atmospheric, the plasmas shrank to stable microplasmas [63]. Though these filaments saturate the camera in the photographs given here, they can be seen with the eye. The array was left at atmospheric pressure for fifteen minutes with the plasma lit. The peak local temperature of the dielectric resonators was $55°C$ at the point where the plasma touched the resonators, which means that the plasma ignited here was cold and non-equilibrium.

As mentioned earlier, no damage was seen on the resonators.

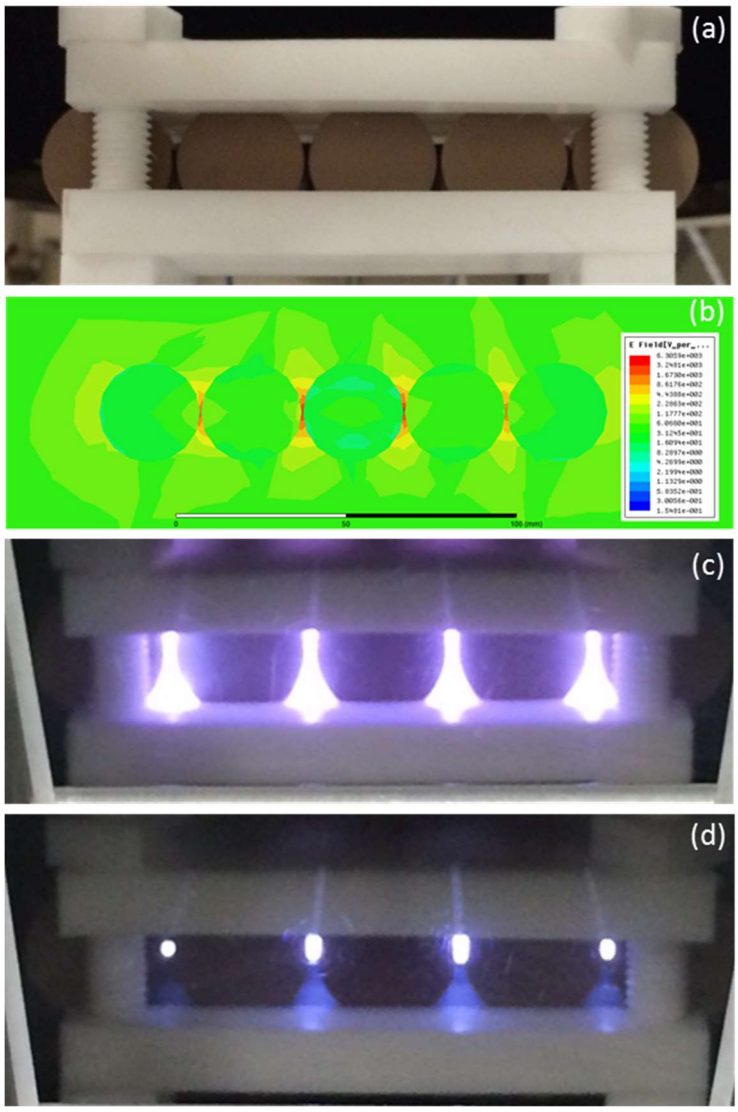

Figure 42: a) Five resonator array, b) Simulated electric field (6.3 kV/m @ 1W), c) Low pressure operation: 0.8 Torr, argon 25 W, d) High pressure operation: 730 Torr, argon 10.5 W [63].

5.2 Reconfigurability

5.2.1 Results of measuring change in reflection/transmission

The two previous chapters demonstrated that an array of dielectric resonators can be used to start plasma elements at low powers. Now we must see if and how the presence of these plasmas change the properties of the overall material.

Two basic experiments were performed with the $CaTiO_3$ resonators. One was just a pair of resonators, and the other was with the array of five resonators. Both demonstrated modulation of the backscattering of the array when plasma was started.

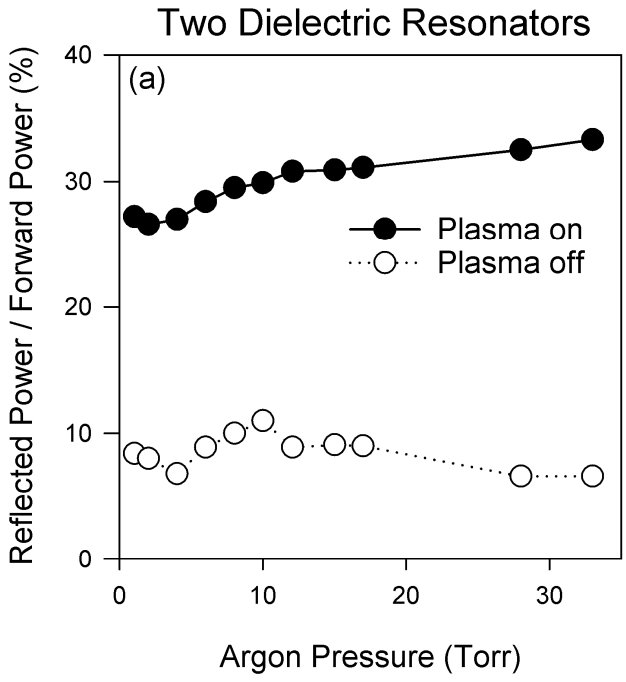

Figure 43: Reflection study with resonator pair, with forward powers as plotted in Figure 41*a.*

The pair of resonators was swept from a pressure of 1 Torr to about 30 Torr. The resonators were separated by a distance of 1 mm. The experimental procedure involved finding an appropriate power level. Then the signal generator was tuned to just below or above resonance. The reflection was measured at this frequency, and then the signal generator was tuned to ignite the plasma, and the new reflection was measured. Then, the plasma was extinguished, and the measurement was begun

at a new pressure. For this experiment, each data point was collected at a different pressure, with a newly ignited plasma for each.

Because reflection measurements were made with percentage of reflection rather than absolute values, a lower power at the same resonance was used rather than changing frequency for reflection measurements.

As shown in Figure 43, when the plasma was not present, the reflection was 10% or less. When the plasma was lit, the reflection jumped up to around 30%.

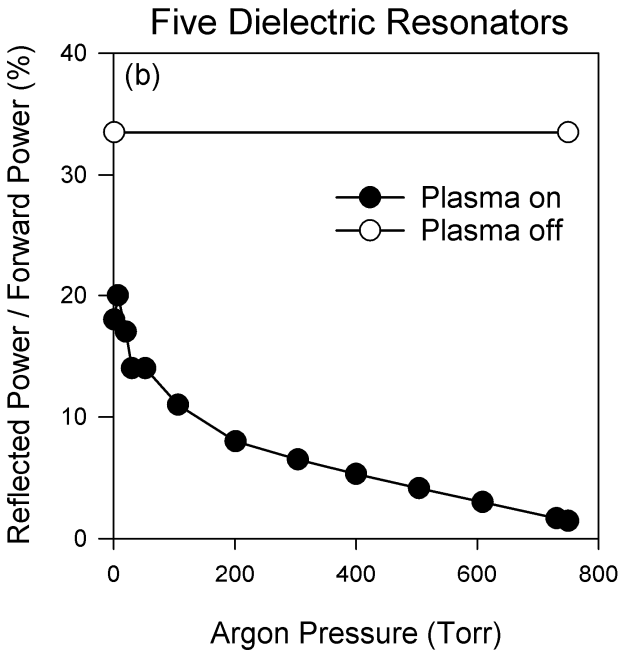

Figure 44: Reflection study with a five-element dielectric array.

The second experiment involved an array of five resonators. For this experiment, the breakdown was initiated and the plasma stayed lit as the pressure was swept from 1 Torr up to 760 Torr, atmospheric pressure. For this experiment, the plasma was begun at a low pressure. Then, the pressure was increased incrementally and

the reflection was measured each time the pressure was increased. This should be distinguished from the previous experiment, which had measurements at a relatively low pressure and narrow range, and had a new plasma for each data point. After the reflection was measured with the plasma on, it was measured with no plasma at the endpoints of the data, at 1 Torr and atmospheric pressure.

The results are shown in Figure 44. When there was no plasma in the array, the reflection was about 33%. When the plasma was ignited at low pressure, the reflection decreased to 20%. As the pressure was increased to atmospheric pressure, the reflection went to as little as 1% [64].

5.2.2 Discussion of change in electromagnetic reflection

Both experiments demonstrated that there was a change in the electromagnetic reflection of the dielectric array when the plasma was ignited. However, since the experiments are distinct and seem to demonstrate conflicting results, I will further discuss their differences and implications.

For the resonator pair, it appears that at this resonant frequency (~1.1 GHz), the resonator pair and Teflon stand are relatively transparent. Each data point was the result of newly ignited plasma, showing that reflection was modulated by the presence of plasma. Even when the dielectric array structure is "off," with no plasma present, it has a low reflection, most likely much lower than if the structure were made of conductive material like copper for the split ring resonators. The increase in reflection demonstrates that the plasma changes the overall scattering of the structure. When the plasma is lit, an impedance appears in between the

resonators and directly in front of the antenna. The plasma is conductive and presents an impedance mismatch that will cause scattering back to the antenna.

Reflected power comes from both the impedance mismatch of the antenna and the 50 Ω power amplifier and the wave scattering off the dielectric resonator array. For this antenna, the ratio of reflection to forward power due to mismatch is usually about 5% [56]. The resonator pair does not offer much more reflection than the antenna mismatch causes, but when the breakdown occurs in low pressure, a large volume of diffuse plasma forms, increasing the reflection.

While the reflection increased for the resonator pair experiments, a seemingly opposite result was obtained with the experiment for the five-resonator array. The reflection decreases when the plasma begins and only continues to decrease as pressure increases. In this experiment, when the plasma is not lit, the array of resonators is reflecting more because it is roughly the same width as the antenna itself. These resonators are forming a radar cross section that is large enough to be "seen" by the ~1 GHz wave. The antenna has a comparable characteristic dimension to the dielectric resonator array and that likely accounts for the higher reflection. When the plasma is lit, a resistance appears in between each of the resonators. As Argon is pumped back into the chamber, increasing the pressure, the density of gas increases and so may the electron density of the plasma. In less dense plasma, the electrons do not have as many collisions and can travel more freely to cancel the electric field. But as the electron density increases, the electron plasma frequency increases as well.

Experiments were not done to measure the electron density, but there are still methods to approximate the qualitative behavior. A finite difference time domain (FDTD) simulation with a self-consistent model was created by José Gregorio and used here with permission. Though it did not model the actual geometry of the experiments, it is instructive as a tool for predicting what may have happened. Gregorio's geometry was a simplified model with a five-element array of resonators with 2 mm gap spacing, but with 2D resonators that were rectangular rather than 3D and cylindrical.

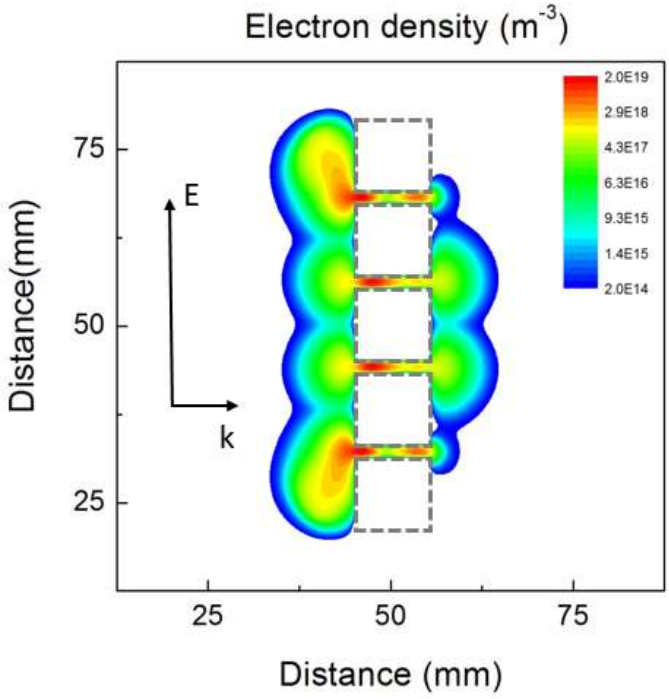

Figure 45: Finite Difference Time Domain (FDTD) simulation of rectangular resonator array.

The simulation calculated that with a 5 kV/m E-field source at 1.5 GHz, the resonators absorbed 0.1 W while the plasma absorbed 16 W. This seems to agree with the observations from the five-resonator array above. If most of the power is

being absorbed by the resonator array and plasma, very little power will reflect back to the source.

This suggests that reflection is decreasing because the plasma is absorbing rather than radiating back the energy. If all of the radiation is absorbed at this resonant frequency, the impedance of the material has been matched to that of free space. If electron density increases, impedance could be increasing as well. The resulting electron density was calculated and Figure 45 plots the electron density for the plasma surrounding the resonators. The peak electron density was higher than 10^{19} m^{-3}, giving an approximate plasma frequency of 28.36 GHz and an estimated plasma permittivity of -350.

The array has low reflection to begin with, and decreases when the plasma is introduced. However, it should be reiterated that this is a rough approximation that does not actually model the experiments described in Chapter 3. It only offers a potential suggestion for why reflection decreases. The simulation does, however, suggest that the plasma permittivity is negative, partially satisfying the requirements for a negative index of refraction metamaterial.

6. Further discussions on dielectric permittivity and electric field

While studying breakdown, I investigated using different materials for dielectric resonators and which properties lend themselves to achieving breakdown. This chapter discusses finding an appropriate permittivity and how electric permittivity is related to the coupled electric field between resonators.

6.1 Motivation for relationship between dielectric permittivity and electric field

Our initial experiments were conducted using cylindrical "hockey pucks" made of calcium titanate ($CaTiO_3$). A permittivity of about 170 and a loss tangent on the order of 10^{-4} were sufficient for locating a suitable mode and igniting plasma, as described and studied in the previous three chapters.

However, three examples suggested that this was a fortunate choice for dielectric material.

From personal correspondence with Adam Chapman in June 2016, I learned that he had tried a similar experiment to that described in Chapter 3, but with resonators made of barium strontium titanate (BaO_4SrTi or BST for short), which has a relative permittivity of $\epsilon_r \sim 800$. The goal of the experiment was exploring whether a higher permittivity material would give stronger coupling and higher resonance frequency. A higher permittivity, which yields a greater discontinuity between the resonator and air, more closely matches a cylindrical cavity resonator. However, this experiment with cylindrical resonators of smaller diameter could not excite plasma.

In a second set of experiments, from personal correspondence in June 2016, Zane Cohick of Pennsylvania State University tried using a split dielectric resonator made of Zirconium Titanate (with permittivity of around 37) in our lab and could not start plasma. Both this experiment and the one started above were conducted in the same lab with similar equipment and setups, but neither was able to reproduce the results of the $CaTiO_3$ experiments.

I then conducted a third set of experiments, trying to achieve breakdown with a new shape and material, spherical resonators of alumina. This geometry could potentially lead to easier expansion to a meta-volume, due to the crystalline stacking of spheres. PSU could not fabricate spheres of $CaTiO_3$, but they recommended ball bearings made of a commercially available dielectric, such as alumina. This would have been very convenient and cost effective as well. Alumina has a relative permittivity of ~11 at its most pure (crystal sapphire or ruby) and ~8 at lower purities. The alumina spheres were arranged in a hexagonal pattern, which simulations had suggested yield strong coupling of the electric field at certain modes.

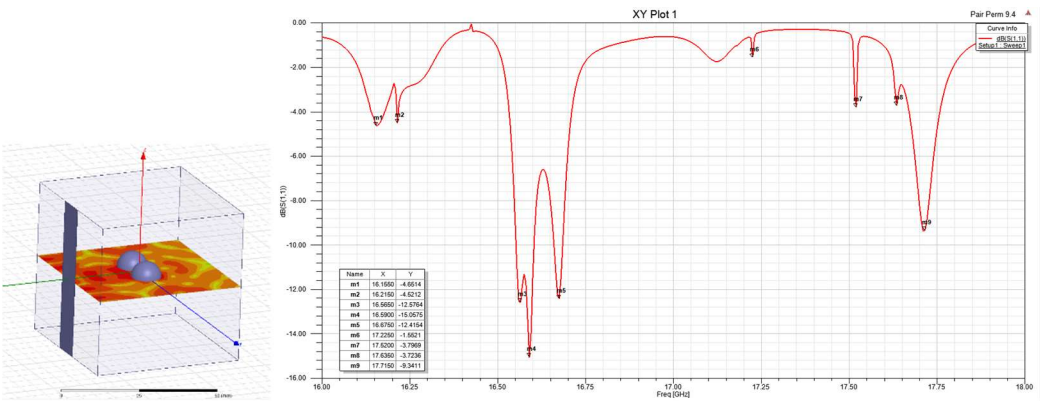

Figure 46: On the left, spherical resonator configuration, on the right, S_{11} curve showing potential resonances.

The alumina ball bearing experiments were also unsuccessful. Materials with permittivities both higher and lower than that of calcium titanate were unsuccessful.

This collection of experiments suggested that calcium titanate had been a good choice for initiating breakdown, but I wanted to confirm this.

One other motivation for this additional experiment was that there could be a permittivity where there would be a maximum field strength. At a permittivity of 1, $\epsilon_r = \epsilon_0$ and there would be no resonator because the dielectric could not be distinguished from free space. But at an infinite permittivity, all fields would be reflected and there would be no resonance. Assuming that electric field is a continuous function of permittivity, since there are roots at two separate points and a non-zero value in between, there must be a maximum value somewhere between the two zeros.

6.2 Method for determining relationship between permittivity and electric field

I wanted to determine and characterize a relationship between electric field and permittivity. The same fundamental simulation described in Chapter 4.3 was modified for these results. I probed the electric field between a pair of resonators of various permittivities, maintaining the same resonant mode (HEM_{111}) as was used in the lab experiments. Two sets of data were taken, first at the same frequency, then at the same resonator diameter.

In order to ensure that the same mode was being excited during each simulation, either the size of the resonator or the frequency of the reference mode had to be

scaled. The reference point was the permittivity of calcium titanate, 165, which was used in the lab experiments. This permittivity was doubled and halved many times up to 1320 and down to 10.3125. The diameter of the resonators scales with the square root of the dielectric. For example, doubling the dielectric constant means that the diameter of the resonator should be divided by square root of two to achieve the same root. To maintain consistency, the electric field strength was measured by HFSS as "Complex_MagE", the scalar magnitude of the complex electric field quantity (essentially, the vector length on a complex plot). Since I was measuring the electric field at the same mode at the same frequency with each variation, the resonator diameters and height, the size of the volume simulated, and the size of the antenna in the simulation were all scaled to ensure consistency across simulations. The loss tangent was kept constant at $5x10^{-4}$.

When this set of experiments with changing diameter was complete, we wanted to make sure that any changes in gap electric field weren't caused by the different sizes of the resonator. To confirm that the gap electric field is a function of permittivity, I also simulated extra cases where resonator diameter was kept constant and the HEM_{111} mode was located at scaled frequencies.

The results can be seen below in Figure 47: Effect of permittivity on electric field strength.

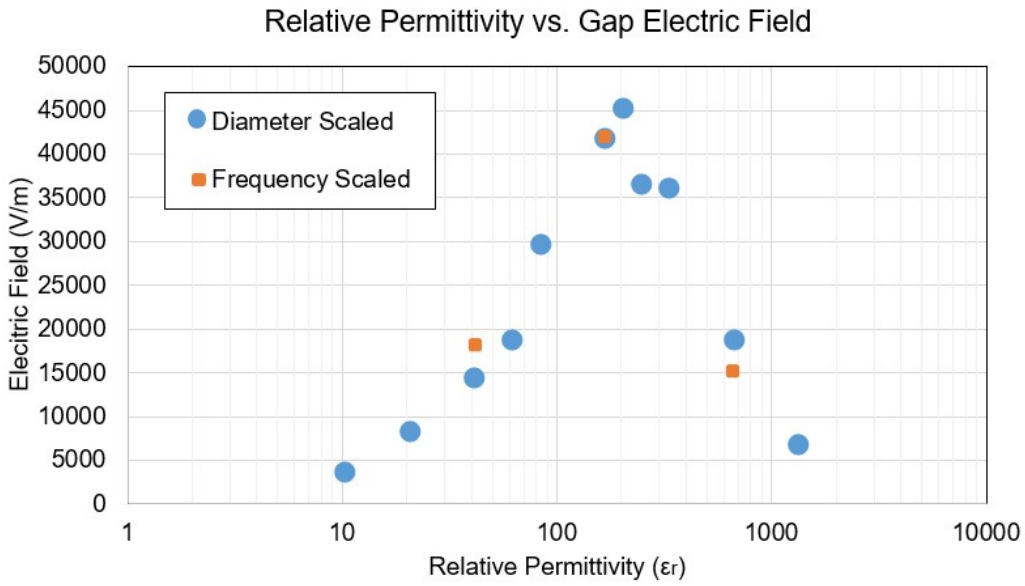

Figure 47: Effect of permittivity on electric field strength.

6.3 Desired dielectric properties

This experiment confirms that the electric field strength in the gap depends on the permittivity of the material. In both cases, scaling the diameter and scaling the frequency of the resonant mode, increasing or decreasing the permittivity by a factor of two decreased the electric field in the gap. The addition of some finer points between 165 and 330 reveals a maximum near $\epsilon_r = 200$.

As the dielectric was changed away from 165, the field strength in the gap (which was always 2 mm) decreased considerably, as much as by two orders of magnitude when $\epsilon_r = 10$.

More points were simulated between 165 and 330 to find the permittivity where maximum fields could be found. Of the two added data points, the highest was 200. Although pure $CaTiO_3$ can achieve the proper electric field strength at low powers, a combination of $CaTiO_3$ and $CaCu_3Ti_4O_{12}$, which has a remarkably high dielectric

of 10,000 but large loss tangent $tan\delta$ at room temperature of 0.15, could potentially reach permittivities closer to $\epsilon_r = 200$, leading to even lower necessary input power [65].

One review of dielectric resonator antennas suggested that dielectric antennas become more broadband as the permittivity decreases [66]. At low permittivity, the resonators are radiating the energy away rather than storing it. Yet at high permittivity, the boundary between free space and the dielectric material is too high, and the fields cannot penetrate the dielectric enough to resonate. Recalling that a dielectric resonator with a very large permittivity resembles a conducting cavity resonator, fields cannot enter a cavity resonator unless there is something inserted into the cavity to perturb the system.

To investigate whether the lower permittivity led to a broader resonance, even with the same loss tangent, I plotted not just the maximum field values as in Figure 47, but the electric field Complex_MagE in the frequency range 1 to 1.2 GHz. Figure 48 shows how as the permittivity increases, the resonance of the HEM_{111} mode not only increases, but becomes more narrow. As the permittivity decreases, the resonances becomes broader, until completely disappearing with a permittivity of 20.625. Similarly broad resonances were seen in the alumina spherical resonators discussed earlier. Those broad resonances were likely due to the lower permittivity of alumina.

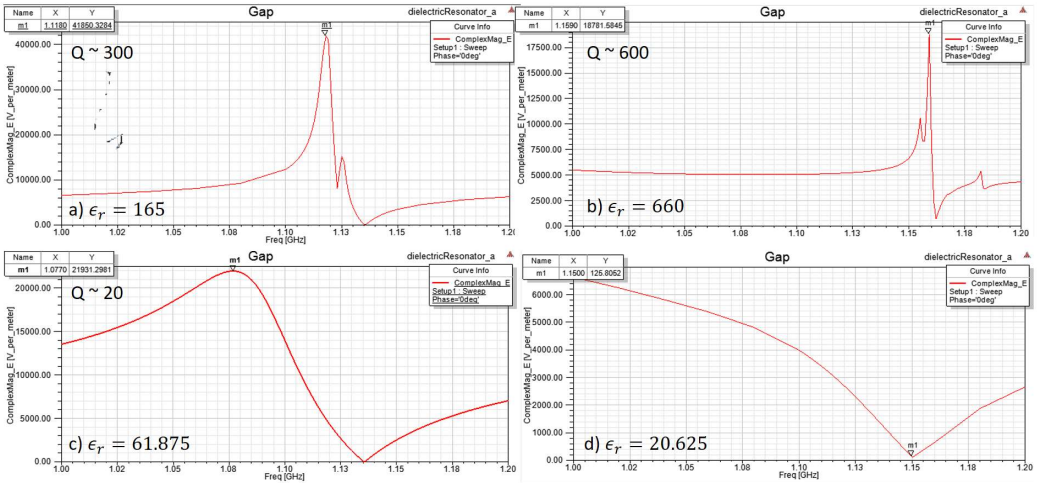

Figure 48: Resonance and Q changing with permittivity: a) $\epsilon_r = 165, Q \sim 300$, b) $\epsilon_r = 660, Q \sim 600$, c) $\epsilon_r = 61.875, Q \sim 20$, d) $\epsilon_r = 20.625, Q\ N/A$.

To confirm that these changes in maximum electric field of the relationship between electric field and the permittivity, independent of the frequency regime, the experiment was also scaled by a factor of ten up to 10 GHz. In these simulations, the resonators were 3 mm in diameter with a gap of 0.2 mm. At $\epsilon_r = 165$, the electric field was 45 kV/m, but when the permittivity was decreased to 41.25 or increased to 660, the field strength dropped to 15 kV/m. This implies that this relationship between permittivity and electric field holds at higher frequencies.

7. Future Work

7.1 Negative index of refraction and metamaterial reconfigurability

The only step towards the construction of a metamaterial was the demonstration that plasma can be started with dielectric resonators. A future step is to show that the permittivity of the plasma is negative at resonance and combine with a negative permeability material in order to have successfully built a negative-index metamaterial. Though the approximation by Gregorio suggested that the plasma could have negative permittivity, there were no experimental confirmations. Some papers hint that I can take advantage of Mie resonances in the dielectric resonator arrays to enhance magnetic resonance [67].

This is how to complete the process of developing a "conductor-less" reconfigurable plasma metamaterial. If we can not only generate plasma with dielectric resonators but guarantee that it has negative permittivity, then we need only combine these with a negative permeability material to achieve a fully left handed material.

There are still challenges beyond this relatively simple proposed material. The incident wave must be at the resonance of the plasma-generating material, but since this frequency is what also sustains breakdown, the frequency at which the plasma starts should also be a frequency where the permittivity of the plasma is negative (i.e., above the electron plasma frequency). Whatever resonator is providing the negative permeability in this proposed metamaterial must also exhibit these properties near this ignition frequency, and this may not be a trivial task. In

addition, though collisions were ignored in the expression for plasma permittivity, they cannot be realistically ignored in all situations. These collisions introduce a loss term that would attenuate a wave even if the plasma had negative permittivity and was combined with a material with negative permeability.

Nonetheless, negative index of refraction metamaterials should be pursued with this material because the plasma could be one way to modulate the behavior of the material. Perhaps when the plasma is not present, waves can pass through the medium in a conventional fashion, but when ignited, the plasma can either redirect the waves at an angle opposite the angle of incidence or attenuate the wave.

In Chapter 2.1, the concept of intrinsic impedance was introduced, along with the idea of perfect absorption. With a metamaterial, it may be possible to create a material with overall permeability and permittivity matching that of free space, ensuring perfect absorption at the matched frequency. The experiments discussed in this thesis demonstrated how the plasma generated could absorb most of the incident radiation, especially at atmospheric pressure. This is an area worth investigating in the future not just for radar cloaking technology but more efficient antennas, transmitters, and receivers.

7.2 Two- and three-dimensional high frequency array structures

Although this thesis demonstrates a successful building block of a one-dimensional meta-surface, the eventual goal is to reach two-dimensional and three-dimensional structures. This would mean achieving, among other things, plasma generation at any angle of incidence.

It may make sense, when moving to a structure in two or three dimensions, to develop arrays with other geometries, such as spheres. And once this modification has been made, it is not that far of a leap to begin designing crystalline structures rather than simple linear arrays.

The next immediate step is two-dimensional arrays. Preliminary simulations with $CaTiO_3$ modeling material suggest that an array of 3x3 resonators, as shown in Figure 49, can achieve high enough field to get breakdown. Important considerations when building a plasma-initiating dielectric array are consistency of resonator size, high (but not too high) permittivity, low pressure with an appropriate gap size, and sufficient power.

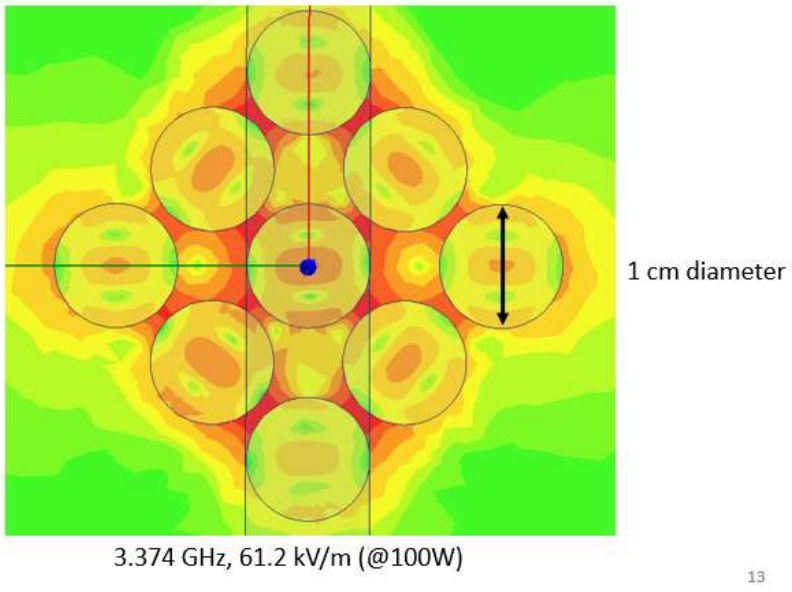

Figure 49: Simulation of electric field in proposed 3x3 resonator array structure

Moving to different geometries, particularly ones that may be easier to consistently manufacture, could make higher frequency materials possible. And although a metamaterial built from these materials at this size is appropriate for microwave

frequencies, there is interest in achieving these results at smaller wavelengths and higher frequencies [68]. By scaling down the material dimensions, we can scale up the frequencies of operation, and try to close the THz gap [11]. One concern is that higher permittivities yield lower frequency operation, as dielectric material increases the size of a wavelength relative to free space. The wave must be larger than the material, so when working with sub milli- or micrometer wavelengths, a resonant structure built of $CaTiO_3$ would need to be very small to reach the same mode.

Potential hurdles include obtaining equipment at the correct frequency or high enough power to initiate breakdown. For this future work, identifying a proper material and resonant mode could be enough to design a meta-surface.

7.3 Plasma properties and behavior

Finally, these experiments did not measure some of the fundamental quantities of plasma. There were no attempts to control the plasma beyond acknowledging that the reflection changes with changing pressure. Future projects should measure the electron density in order to determine other important properties like electron plasma frequency. This could be a way to demonstrate, as mentioned in Chapter 7.1, that the plasma permittivity was negative.

8. Conclusions

Plasma was successfully generated with arrays of dielectric resonators. I identified important properties or characteristics for starting the plasma, including pressure, resonator separation gap size, and input power. However, the "go, no-go" for starting plasma was the relative permittivity of the material. The experiment was only successful with resonators made of calcium titanate, which has a relative permittivity of about 167. Resonators made of materials with considerably lower (<40) or higher permittivities (>800) could not start plasma. A simulation study suggests that a maximum occurs around a permittivity of 200. Calcium titanate is a material in this optimal range for breakdown.

The plasma was started in argon near 1.1 GHz, the HEM_{111} resonance for the resonators, with separations between 0.5 mm and 5 mm.

I also demonstrated that the electromagnetic scattering of the array could be modulated. The reflection changed depending on if the plasma was present or not. Physically small arrays had increases in reflection while larger arrays had decreases in reflection. Furthermore, changing the pressure of the system changed the reflection. Though plasma had to be ignited at relatively low pressures, once the plasma was lit, increasing the system to atmospheric pressure decreased reflection to the antenna to 1%.

It should be noted that electron density was never measured, and that some of the experimental methods could have been improved, such as using a vector network analyzer instead of a manual frequency sweep. As such, this is only the beginning

of research on plasma reconfigurable metamaterials and how dielectric resonators can be used to break down gas.

Future work should focus on developing a surface of microplasma and dielectric resonators in two dimensions and exploring alternate geometries, materials, and frequencies. However, the most important next step may be to prove that I have achieved negative permittivity with the plasma and determine whether negative permeability can be reached with the dielectric resonators. The “passively” started or self-ignited plasma generators, in conjunction with low input power and reflection needed to start and sustain plasma, suggests great potential for cloaking using the metamaterial’s modulation of backscattering.

9. Appendix

Mode study:

TE_{011} Mode – 0.8026 GHz

E Field:

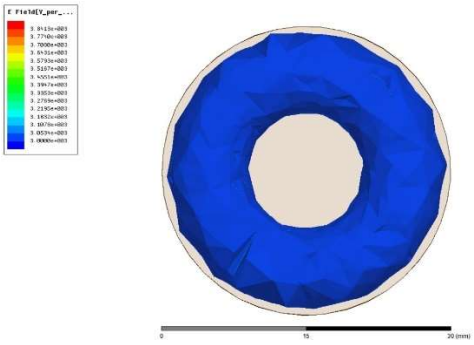

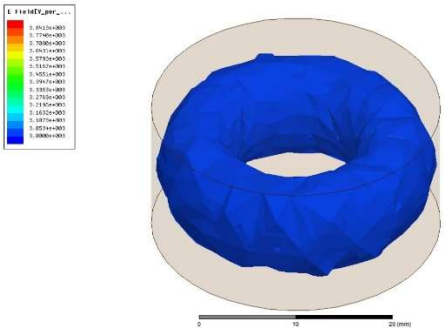

H Field:

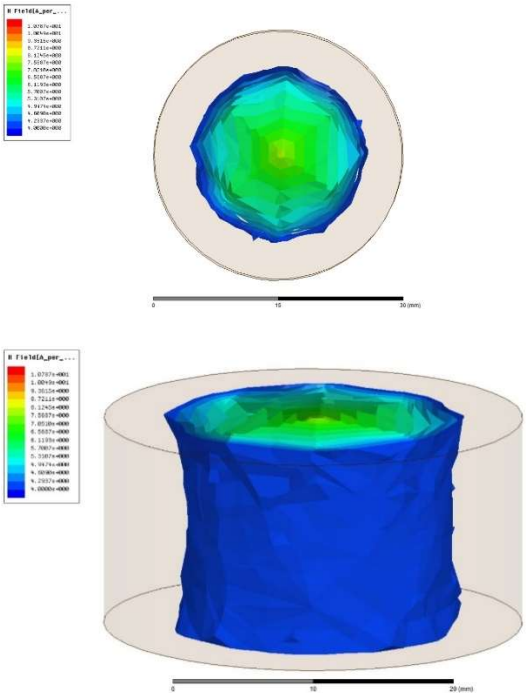

HEM_{111} – 1.1145 GHz

E Field:

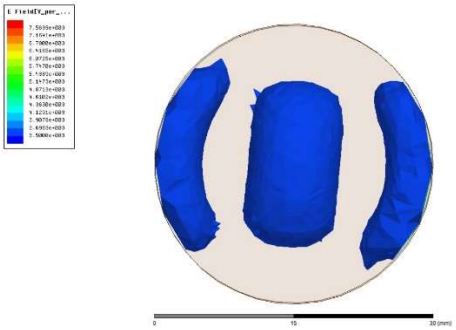

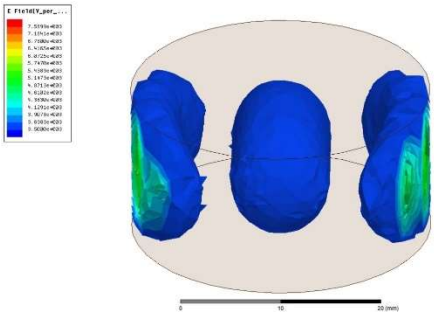

H Field:

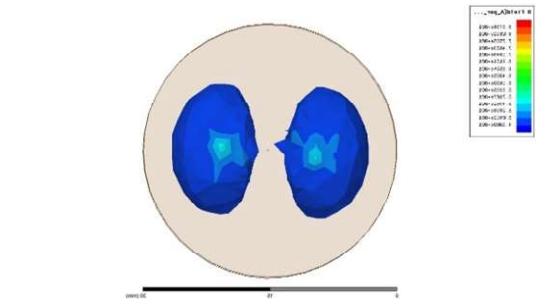

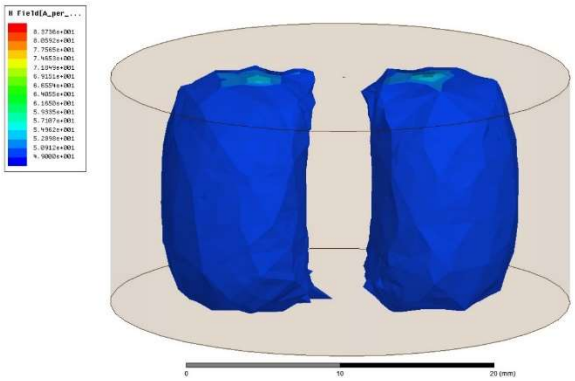

10. References

[1] J. B. Pendry, A. J. Holden, D. J. Robbins and W. J. Stewart, "Magnetism From Conductors And Enhanced Nonlinear Phenomena," *IEEE Transactions On Microwave Theory And Techniques,* vol. 47, no. 11, pp. 2075-2974, November 1999.

[2] D. R. Smith, W. J. Padilla, D. C. Vier, S. C. Nemat-Nasser and S. Schultz, "Composite medium with simultaneously negative permeability and permittivity," *Physical Review Letters,* vol. 84, no. 18, pp. 4184-4187, 1 May 2000.

[3] D. R. Smith and N. Kroll, "Negative refractive index in left-handed materials," *Physical Review Letters,* vol. 85, no. 14, pp. 2933-2936, 17 May 2000.

[4] P. K. Singh, J. Hopwood and S. Sonkusale, "Metamaterials for Remote Generation of Spatially Controllable Two Dimensional Array of Microplasma," *Scientific Reports,* vol. 4, no. Article number: 5964, 2014.

[5] C. Caloz and T. Itoh, Electromagnetic Metamaterials: Transmission Line Theory and Microwave Applications, Wiley-IEEE Press, 2006.

[6] D. Griffiths, Introduction to Electrodynamics, 4th ed., Pearson, 2013.

[7] A. Guth and M. Chen, *8.07 E,* Massachusetts Institute of Technology: MIT OpenCourseWare, Fall 2012.

[8] V. G. Veselago, "THE ELECTRODYNAMICS OF SUBSTANCES WITH SIMULTANEOUSLY NEGATIVE Values of Epsilon and Mu," *Soviet Physics USPEKHI,* vol. 10, no. 4, pp. 509-514, 1968.

[9] J. R. Minkel, "Focus: Left-Handed Materials Debate Heats Up," *Physics Review Focus,* vol. 9, no. 23, 2002.

[10] D. M. Pozar, "Microwave Engineering," 4th ed., John Wiley & Sons, 2012.

[11] C. Sitori, "Bridge For The Terahertz Gap," *Nature,* vol. 417, 9 May 2002.

[12] H. Conrads and M. Schmidt, "Plasma Generation and Plasma Sources," *Plasma Sources Science and Technology,* pp. 441-454, 2000.

[13] M. A. Lieberman and A. J. Lichtenberg, Principles Of Plasma Discharges And Materials Processing, 2nd ed., Hoboken, NJ: John Wiley & Songs, Inc., 2005.

[14] P. PaneerChelvam, L. L. Raja and R. R. Upadhyay, "Computational modeling of a single microdischarge and its interactions with high frequency electromagnetic waves," *Journal of Physics D: Applied Physics,* vol. 49, 2016.

[15] F. Iza and J. Hopwood, "Split-ring Resonator Microplasma: Microwave Model, Plasma Impedance and Power Efficiency," *Plasma Sources Science and Technology,* vol. 14, pp. 397-406, 2005.

[16] J. Hopwood, A. R. Hoskinson and J. Gregorio, "Microplasmas ignited and sustained by microwaves," *Plasma Sources Science and Technology,* vol. 23, Dec. 2014.

[17] A. R. Hoskinson and J. Hopwood, "A two-dimensional array of microplasmas generated using microwave resonators," *Plasma Sources Science and Technology,* vol. 21, July 2012.

[18] J. Gregorio, S. Parsons and J. Hopwood, "Microwave harmonic generation and nonlinearity in microplasmas," *Plasma Sources Science and Technology,* 2016.

[19] S. Fiedziuszko, I. Hunter, T. Itoh, Y. Kobayashi, T. Nishikawa, S. Stitzer and K. Wakino, "Dielectric Materials, Devices, and Circuits," *IEEE Transactions on Microwave Theory and Techniques,* vol. 50, no. 3, pp. 706-719, 2002.

[20] R. D. Richtmyer, "Dielectric Resonators," *Journal of Applied Physics,* vol. 10, pp. 391-398, June 1939.

[21] Skyworks Solutions, "Tuning and Exciting Dielectric Resonator Modes," Trans Tech, Inc., Adamstown, MD, 2007.

[22] M. Iwasaki, E. Semouchkina, G. B. Semouchkin, K. Z. Rajab, C. A. Randall and M. T. Lanagan, "Symmetry Matching of Hybrid Modes for Dielectric Materials," *Japanese Journal of Applied Physics,* pp. 2835-2841, 2006.

[23] L. f. I. Research, "Tables of Dielectric Materials Volume IV," Massachusetts Institute of Technology, Cambridge, MA, 1953.

[24] W. B. Westphal and A. Sils., "Dielectric Constant and Loss Data, Vol. IV," Air Force Materials Laboratory, ?, 1972.

[25] T. Luo, B. Li, Q. Zhao and J. Zhou, "Dielectric Behavior of Low Microwave Loss Unit Cell for All Dielectric Metamaterial," *International Journal of Antennas and Propagation,* 2015.

[26] S. Kucheiko, J. Choi, H. Kim and H. Jung, "Microwave Dielectric Properties of CaTiO3-Ca(Al1/2Ta1/2)O3 Ceramics," *Communications of the American Ceramic Society,* vol. 79, 1996.

[27] S. Sahoo, S. K. S. Parashar and S. M. Ali, "CaTiO3 Nano Ceramic For NTCR Thermistor Based Sensor Application," *Journal of Advanced Ceramics,* pp. 117-124, 2014.

[28] T. Liu, X. Zhao and W. Chen, "A/B Site Modified CaTiO3 Dielectric Ceramics For Microwave Application," *Journal of the American Ceramic Society,* pp. 1153-1155, 2006.

[29] J. P. Turpin, J. A. Bossard, K. L. Morgan, D. H. Werner and P. L. Werner, "Reconfigurable and Tunable Metamaterials: A Review of the Theory and Applications," *International Journal of Antennas and Propagation,* 2014.

[30] H. Tao, A. C. Strikwerda, K. Fan, W. J. Padilla, X. Zhang and R. D. Averitt, "Reconfigurable Terahertz Metamaterials," *Physical Review Metamaterials,* vol. 103, 2009.

[31] J. P. Turpin, D. H. Werner and D. E. Wolfe, "Design Considerations for Spatially Reconfigurable Metamaterials," *IEEE Transactions On Antennas And Propagation,* vol. 63, no. 8, pp. 3513-3521, 2015.

[32] Fujitsu Microelectronics America, Inc., "Fundamentals of Liquid Crystal Displays - How They Work and What They Do," Sunnyvale, CA, 2006.

[33] B. Guo, "Negative refraction in the terahertz region by using plasma metamaterials," *Journal of Electromagnetic Waves and Applications,* vol. 26, no. 17-18, pp. 2445-2451, 2012.

[34] O. Sakai and K. Tachibana, "Plasmas as metamaterials: a review," *Plasma Sources Science and Technology,* vol. 21, no. 1, 2012.

[35] H. Mehdian, Z. Mohammadzahery and A. Hasanbeigi, "Optical and magneto-optical properties of plasma-magnetic metamaterials," *Journal of Physics D: Applied Physics,* vol. 48, no. 30, 2015.

[36] S. Zhang, Y. Xiong, G. Bartal, X. Yin and X. Zhang, "Magnetized Plasma for Reconfigurable Subdiffraction Imaging," *Physical Review Letters,* vol. 106, 2011.

[37] I. V. Shradrivov, M. Lapine and Y. S. Kivshar, Eds., Nonlinear, Tunable, and Active Metamaterials, Springer Publishing, 2015.

[38] C. H. Liu and N. Behdad, "Plasma-tunable metamaterials and periodic structures," in *Vacuum Electronics Conference (IVEC), 2013 IEEE 14th International*, Paris, 2013.

[39] N. Michishita, T. Mori, S. Kamada and Y. Yamada, "Dielectric metamaterial lens antenna for wide angle beam scanning," in *2010 IEEE International Conference on Wireless Information Technology and Systems (ICWITS 2010)*, Honolulu, HI, USA, 2010.

[40] L. Li, J. Wang, H. Ma, J. Wang, M. Feng, H. Du, M. Yan, J. Zhang, S. Qu and Z. Xu, "Achieving all-dielectric metamaterial band-pass frequency selective surface via high-permittivity ceramics," *Applied Physics Letters,* vol. 108, no. 12, 21 March 2016.

[41] J. Wang, Z. Xu, Z. Yu, X. Wei, Y. Yang, J. Wang and S. Qu, "Experimental realization of all-dielectric composite cubes/rods left-handed metamaterial," *Journal of Applied Physics,* vol. 109, no. 8, 2011.

[42] T. Lepetit, E. Akmansoy, M. Pate and J.-P. Ganne, "Broadband negative magnetism from all-dielectric metamaterial," *Electronics Letters,* vol. 44, no. 19, 11 Sept. 2008.

[43] S. Remillard, A. Hardaway, B. Mork, J. Gilliland and J. Gibbs, "Using a Re-Entrant Microwave Resonator to Measure and Model the Dielectric Breakdown Electric Field of Gases," *Progress In Electromagnetics Research B,* vol. 15, pp. 175-195, 2009.

[44] B. Zarghooni, A. Dadgarpour and T. A. Denidni, "Reconfigurable metamaterial dipole antenna," in *2014 IEEE International Symposium on Antennas and Propagation & USNC/URSI National Radio Science Meeting*, Memphis, TN, USA, 2014.

[45] Z. Cohick, W. Luo, D. Wolfe, M. Lanagan and J. Hopwood, "Split-post dielectric resonator plasma generators," in *2016 IEEE International Conference on Plasma Science (ICOPS)*, Banff, AB, Canada, 2016.

[46] K. Kourtzanidis, D. M. Pederson and L. L. Raja, "Electromagnetic wave energy flow control with a tunable and reconfigurable coupled plasma split-ring resonator metamaterial: A study of basic conditions and configurations," *Journal of Applied Physics,* vol. 119, no. 20, 28 May 2016.

[47] O. Sakai, A. Iwai and Y. Nakamura, "Plasma metamaterials, and their reconfigurable and nonlinear properties," in *2015 9th European Conference on Antennas and Propagation (EuCAP)*, Lisbon, 2015.

[48] O. Sakai, S. Yamaguchi, A. Bambina, A. Iwai, Y. Nakamura, Y. Tamayama and S. Miyagi, "Plasma metamaterials as cloaking and nonlinear media," *Plasma Physics and Controlled Fusion,* vol. 59, 2017.

[49] Y. Tamayama and O. Sakai, "Microplasma generation by slow microwave in an electromagnetically induced transparency-like metasurface," *Journal of Applied Physics,* vol. 121, 2017.

[50] R. Fleury, F. Monticone and A. Alu, "Invisibility and Cloaking: Origins, Present, and Future Perspectives," *Physical Review Applied,* vol. 4, 2015.

[51] D. Schurig, J. J. Mock, B. J. Justice, S. A. Cummer, J. B. Pendry, A. F. Starr and D. R. Smith, "Metamaterial electromagnetic cloak at microwave frequencies," Sciencexpress, 2006.

[52] Kurt J. Lesker Company, "Vacuum Pumps," [Online]. Available: https://www.lesker.com/newweb/vacuum_pumps/vacuumpumps_technicalnotes_1.cfm. [Accessed 7 October 2016].

[53] M. Moravej, X. Yang, G. R. Nowling, J. P. Chang, R. F. Hicks and S. E. Babayan, "Physics of high-pressure helium and argon radio-frequency plasmas," *Journal of Applied Physics,* vol. 96, no. 12, 2004.

[54] R. E. Bickering, "Fundamentals of Pressure Sensor Technology," *Sensors Online,* 1 November 1998.

[55] S. Carter, A. Ned, J. Chivers and A. Bemis, "Selecting Piezoresistive vs. Piezoelectric Pressure Transducers," Kulite Semiconductor Products, Inc..

[56] Com-Power Corporation, "Double Ridge Horn Antenna AH-118," 2015. [Online]. Available: http://www.com-power.com/datasheets/AH-118.pdf. [Accessed 22 January 2017].

[57] B. Hyland, "Impact of Cable Losses," Maxim Integrated Products, 2008.

[58] B. W. Hakki and P. D. Coleman, "A Dielectric Resonator Method of Measuring Inductive Capacities in the Millimeter Range," *IRE Transactions On Microwave Theory And Techniques,* pp. 402-410, July 1960.

[59] A. G. Cockbain, "Ceramic dielectrics with controlled temperature coefficients of permittivity," *Proceedings of the Institution of Electrical Engineers,* vol. 112, no. 7, pp. 1478-1481, 1965.

[60] R. C. Kell, A. C. Greenham and G. C. E. Olds, "High-Permittivity Temperature-Stable Ceramic Dielectrics with Low Microwave Loss," *Journal of The American Ceramic Society,* pp. 352-354, 1973.

[61] S. Sahoo, U. Dash, S. K. S. Parashar and S. M. Ali, "Frequency And Temperature Dependent Characteristics Of CaTiO3 Nano-Ceramic Prepared By High-Energy Ball Milling," *Journal of Advanced Ceramics,* pp. 291-300, 2013.

[62] C. Torres, P. G. Reyes, F. Castillo and H. Martinez, "Paschen law For Argon Glow Discharge," in *14th Latin American Workshop on Plasma Physics*, 2011.

[63] F. Iza and J. Hopwood, "Atmospheric and High Pressure Plasmas-Self-Organized Filaments, Striations and Other Nonuniformities in Nonthermal Atmospheric Microwave Excited Microdischarges," *IEEE Transactions on Plasma Science,* vol. 33, no. 2, pp. 306-307, 2005.

[64] S. Dennison, A. Chapman, W. Luo, M. Lanagan and J. Hopwood, "Plasma generation by dielectric resonator arrays," *Plasma Sources Science and Technology,* vol. 25, no. 3, 2016.

[65] W. Kobayashi and I. Terasaki, "Ca Cu 3 Ti 4 O 12 / Ca Ti O 3 composite dielectrics: Ba/Pb -free Dielectric Ceramics With High Dielectric Constants," *Applied Physics Letters,* vol. 87, 2005.

[66] A. Petosa and A. Ittipiboon, "Dielectric Resonator Antennas: A Historical Review and the Current State of the Art," *IEEE Antennas and Propagation Magazine,* vol. 52, no. 5, pp. 91-116, October 2010.

[67] Q. Zhao, J. Zhou, F. Zhang and D. Lippens, "Mie Resonance-Based Dielectric Metamaterials," *Materials Today,* vol. 12, no. 12, 2009.

[68] K. Z. Rajab, R. Mittra, M. Naftaly, E. H. Linfield and M. T. Lanagan, "Terahertz transmission through periodic arrays of dielectric and conducting

spheres," in *2007 IEEE Antennas and Propagation Society International Symposium*, Honolulu, HI, 2007.

[69] M. W. Pospieszalski, "Cylindrical Dielectric Resonators and Their Applications in TEM Line Microwave Circuits," *IEE Transactions on Microwave Theory and Techniques,* pp. 233-238, 1979.

[70] H. Kagata and K. Junichi, "Dielectric Properties of Ca-Based Complex Perovskite at Microwave Frequencies," *Japanese Journal of Applied Physics,* vol. 33, pp. 5463-5465, 1994.

[71] J. Ravez, C. Broustera and A. Simon, "Lead-free Feerroelectric Relaxor Ceramics in the BaTiO3-BaZrO3-CaTiO3 system," *Journal of Materials Chemistry,* vol. 9, pp. 1608-1613, 1999.

[72] D. R. Smith, W. J. Padilla, D. C. Vier, S. C. Nemat-Nasser and S. Schultz, "Composite medium with simultaneously negative permeability and permittivity," *Physical Review Letters,* vol. 84, no. 18, pp. 4184-4187, 1 May 2000.

[73] Z. Chen and S. Okamura, "Properties of Dielectric Ring Resonator and Application to Moisture Measurement," *Subsurface Sensing Technologies and Applications,* pp. 203-216, 2002.

[74] M. H. Jones and H. Jones Stephen, "The General Properties of Si, Ge, SiGe, SiO2 and Si3N4," Virginia Semiconductor, 2002.

[75] D. A. Pawlak, "Metamaterials and photonic crystals – potential applications for self-organized eutectic micro- and nanostructures," *Scientia Plena,* vol. 4, no. 1, 2008.

[76] H. Butt, Q. Dai, N. Lal, T. Wilkinson, J. Baumberg and G. Amaratunga, "Metamaterial filter for the near-visible spectrum," *Applied Physics Letters,* vol. 101, no. 8, 2012.

[77] J. M. e. a. Le Floch, "Invited Article: Dielectric material characterization techniques and designs of high-Q resonators for applications from micro to millimeter-waves frequencies applicable at room and cryogenic temperatures," *Review of Scientific Instruments,* vol. 85.3, 2014.

[78] B. Wang and M. A. Cappelli, "Waveguiding and bending modes in a plasma photonic crystal bandgap device," *AIP Advances,* 2016.

[79] Z. Cohick, W. Luo, S. Perini, A. Baker, D. Wolfe and M. Lanagan, "A Novel, All-Dielectic, Microwave Plasma Generator Towards Development Of Plasma Metamaterials," *Applied Physics Express,* vol. 9, 2016.